Stem Cell Reports
Article

OPEN ACCESS

Studies in an Early Development Window Unveils a Severe HSC Defect in both Murine and Human Fanconi Anemia

Carine Domenech,[1,2,3,4,11] Loïc Maillard,[1,2,3,4] Alix Rousseau,[4,5] Fabien Guidez,[3,4] Laurence Petit,[1,2] Marika Pla,[3,4] Denis Clay,[6,7] Fabien Guimiot,[8] Sandra Sanfilippo,[1,2,12] Sebastien Jacques,[9] Pierre de la Grange,[10] Noémie Robil,[10] Jean Soulier,[4,5] and Michèle Souyri[1,2,3,4,*]

[1]CNRS UMR7622/IBPS, Paris, France
[2]Université Pierre et Marie Curie, Sorbonne Universités, Paris, France
[3]INSERM UMR_S1131, Hôpital Saint Louis, Paris, France
[4]IUH, Université Paris Diderot, Sorbonne Paris Cité, Paris, France
[5]INSERM U944/CNRS UMR7212, Hôpital Saint Louis, Paris, France
[6]INSERM U972, Hôpital Paul Brousse, Villejuif, France
[7]Plateforme de cytométrie, UMS33, Université Paris Sud, Villejuif, France
[8]Service de Foetopathologie, Hôpital Robert Debré, Paris, France
[9]Genom'ic, Hôpital Cochin, Université Paris Descartes, Paris, France
[10]GenoSplice Technology, Paris, France
[11]Present address: Institut d'Hématologie et d'Oncologie Pédiatrique, Université Lyon 1, Lyon, France
[12]Present address: Aenitis Technologies, Hôpital Saint Louis, Paris, France
*Correspondence: michele.souyri@inserm.fr
https://doi.org/10.1016/j.stemcr.2018.10.001

SUMMARY

Fanconi anemia (FA) causes bone marrow failure early during childhood, and recent studies indicate that a hematopoietic defect could begin *in utero*. We performed a unique kinetics study of hematopoiesis in *Fancg*$^{-/-}$ mouse embryos, between the early embryonic day 11.5 (E11.5) to E12.5 developmental window (when the highest level of hematopoietic stem cells [HSC] amplification takes place) and E14.5. This study reveals a deep HSC defect with exhaustion of proliferative and self-renewal capacities very early during development, together with severe FA clinical and biological manifestations, which are mitigated at E14.5 due to compensatory mechanisms that help to ensure survival of *Fancg*$^{-/-}$ embryos. It also reports that a deep HSC defect is also observed during human FA development, and that human FA fetal liver (FL) HSCs present a transcriptome profile similar to that of mouse E12.5 *Fancg*$^{-/-}$ FL HSCs. Altogether, our results highlight that early mouse FL could represent a good alternative model for studying Fanconi pathology.

INTRODUCTION

In children, bone marrow failure (BMF) represents a life-threatening condition whose most common genetic cause is Fanconi anemia (FA). FA is a genetic disorder due to mutations in one of the 22 FANC complementation group genes involved in DNA repair and prevention of cellular stress (Bluteau et al., 2016; Deans and West, 2011; Dong et al., 2015; Hays, 2012; Kim et al., 2012; Knies et al., 2017; Kottemann and Smogorzewska, 2013; Kupfer, 2013; Park et al., 2016; Zhang et al., 2015). Early during childhood (median age 6.5 years) (Dokal and Vulliamy, 2008; Faivre et al., 2000; Kutler et al., 2003), 80% of the FA patients suffer from this main symptom (Kutler et al., 2003) and hematopoietic stem cell (HSC) transplantation remains the only curative treatment (Ayas et al., 2013; Peffault de Latour et al., 2013). Furthermore, FA also strongly predisposes patients to myelodysplastic syndrome and acute myeloid leukemia (AML). To date, the pathogenesis of BMF and AML remains incompletely understood (Dumitriu and Young, 2012; Garaycoechea and Patel, 2014; Muller and Williams, 2009; Nalepa and Clapp, 2014; Quentin et al., 2011; Tischkowitz and Dokal, 2004; Walter et al., 2015; Zhang et al., 2016).

Most of the time, FA patients do not show any signs of blood cytopenia at birth (Soulier, 2011). However, a deficit in the CD34^{+} cell numbers in FA subjects is observed very early during childhood, even before the onset of the BMF clinical symptoms (Ceccaldi et al., 2012; Kelly et al., 2007). This, added to the early developmental defects of the hematopoietic commitment described for human embryonic stem cells after knockdown of *FANCA* and *FANCD2* genes, led us and others to hypothesize that the FA hematopoietic defect could already begin *in utero* (Ceccaldi et al., 2012; Kamimae-Lanning et al., 2013; Suzuki et al., 2017; Tulpule et al., 2010; Yoon et al., 2016).

Indeed, in contrast to adult HSCs, which are quiescent in the bone marrow (BM), embryonic HSCs are in active proliferation and migrate through multiple anatomical sites before they settle in the BM (Dzierzak and Speck, 2008; Mikkola and Orkin, 2006). In the mouse, between the time of their emergence in the floor of dorsal aorta in the aorta/gonad/mesonephros (AGM) region and the colonization of BM, HSCs migrate through fetal liver (FL) and placenta (Pl), where they are amplified (Dzierzak and Speck, 2008). Amplification takes place between embryonic day 11.5 (E11.5) and E15.5 in the FL (Ema and Nakauchi, 2000; Kumaravelu et al., 2002; Morrison et al., 1995),

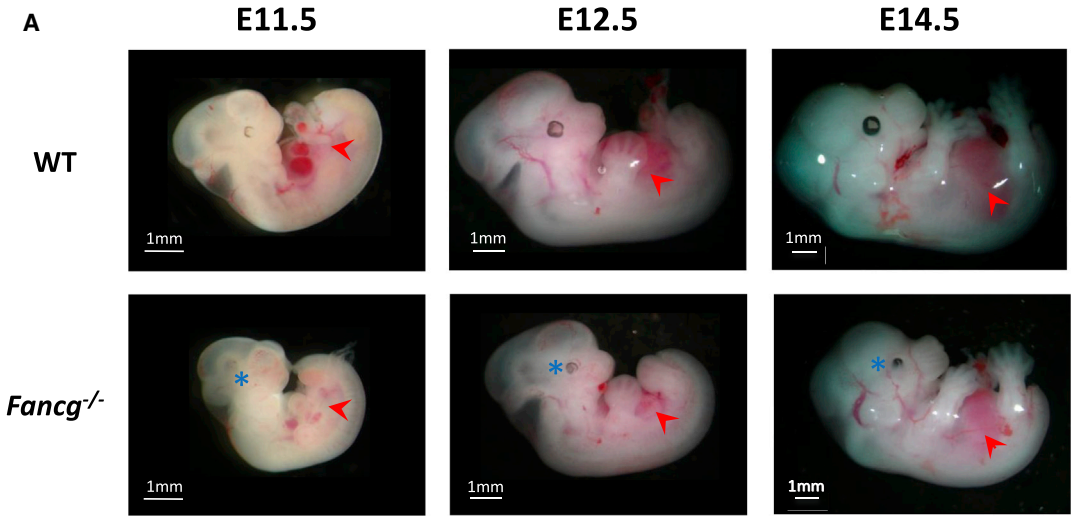

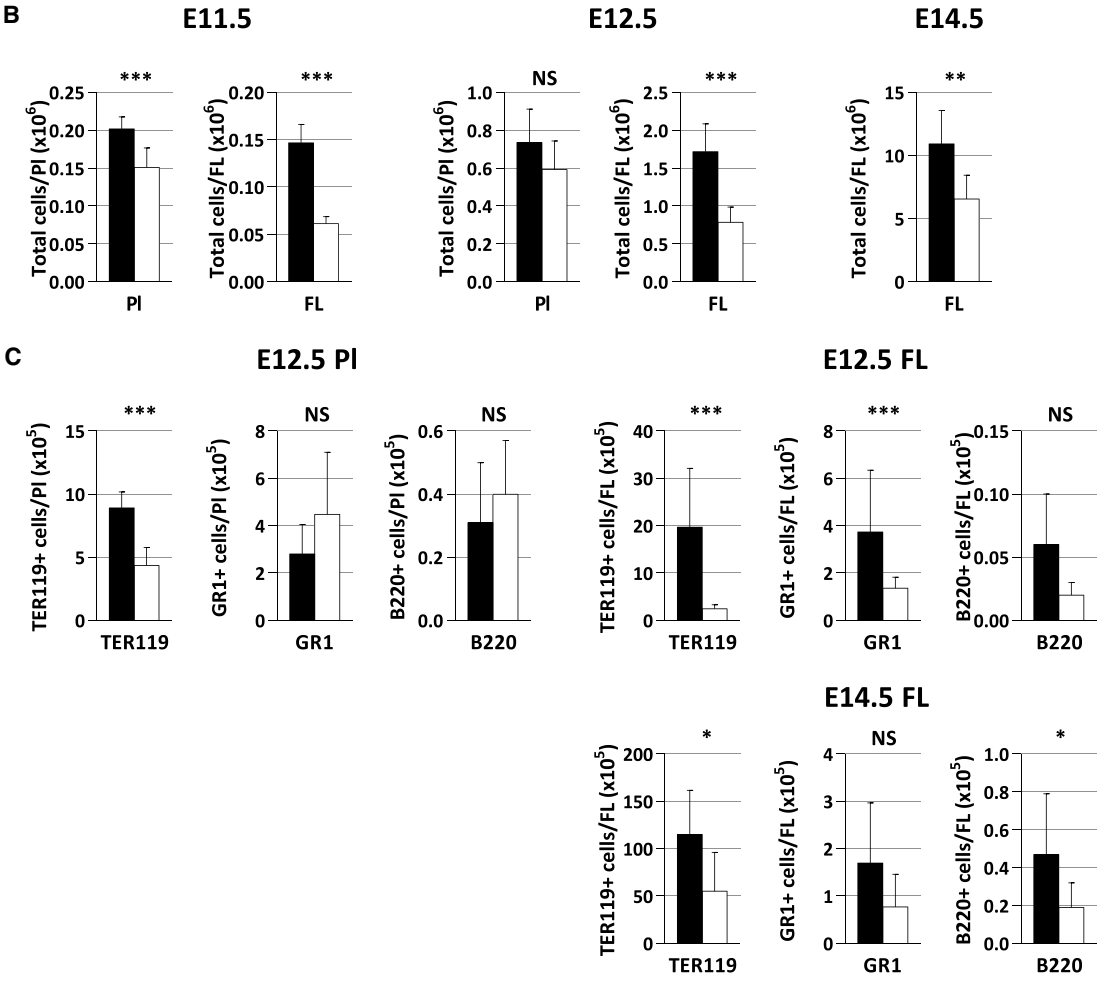

(legend on next page)

with a peak at E12.5 (30- to 50-fold increase between E11.5 and E12.5) (Gekas et al., 2005; Kumaravelu et al., 2002), and between E11.5 and E12.5 in the Pl (25-fold) (Gekas et al., 2005; Ottersbach and Dzierzak, 2005). During human embryonic development, the sequence of events leading to production of HSCs parallels that of mice, and FL represents the key organ for HSC amplification and maturation (Tavian and Peault, 2005).

In this study, we investigated whether FA pathway deficiency impairs the expansion of the HSC pool in response to high replicative stress during the first stages of HSC amplification during embryonic development, using *Fancg*$^{-/-}$ mice. Together with *FANCA* and *FANCC*, *FANCG* is one of the most frequently mutated gene in FA patients, and its product is part of the nuclear FA core complex that signals the cellular response to DNA damage (Dong et al., 2015). Adult *Fancg*$^{-/-}$ mice present a phenotype virtually identical to that of *Fanca*$^{-/-}$ and *Fancc*$^{-/-}$ mice (Parmar et al., 2009), with a reduction of BM HSCs and hematopoietic progenitor (HP) subsets but no BMF (Barroca et al., 2012).

We focused on early development times, when HSC amplification takes place both in FL and Pl, i.e., E11.5–E12.5. At E12.5 expansion is important in both organs, and any DNA repair defect would have a significant impact leading to an alteration of HSC pool. Our results demonstrate that an important hematopoietic defect occurs from the very first stages of hematopoietic amplification in *Fancg*$^{-/-}$ FL and Pl, and that clinical and biological compensations occur at E14.5. In addition, we show that an HSC defect is also present in an FL sample from a human FA embryo. Transcriptomic analysis of HSCs sorted from *Fancg*$^{-/-}$ E12.5 and from the human FA FLs revealed that similar biological processes are down- and upregulated in Fanconi HSCs.

RESULTS

Fancg Deficiency Leads to Impaired Phenotype and Profound Erythrocyte Defect in Fetal Liver and Placenta during Early Mouse Embryonic Development

Fancg$^{-/-}$ homozygous mice being hypofertile (Koomen et al., 2002), embryos were obtained after timed mating of C57Bl6 *Fancg*$^{+/-}$ heterozygous breeders. *Fancg*$^{-/-}$ embryos were obtained at a lower frequency than expected at E11.5 and E12.5 (20% and 21.7%, respectively, instead of 25%, 958 embryos tested in total; $p < 0.001$). As observed in *Fancc*$^{-/-}$ and *Fancd2*$^{-/-}$ mice (Kamimae-Lanning et al., 2013; Suzuki et al., 2017), this frequency dramatically declined at birth (11% ± 0.8, 82 postnatal day 0 [P0] to P1 pups tested, $p < 0.001$), suggesting a late perinatal lethality. Interestingly, at E11.5 and E12.5 *Fancg*$^{-/-}$ embryos were systematically smaller than wild-type (WT) control littermates, while at E14.5 only half of the *Fancg*$^{-/-}$ embryos remained smaller than control (Figure 1A). This size difference between *Fancg*$^{-/-}$ and WT embryos became less pronounced around birth. Eye defects, such as anophthalmia or microphthalmia, were observed in *Fancg*$^{-/-}$ embryos at all stages of development studied (Figure 1A).

FLs of all *Fancg*$^{-/-}$ embryos were systematically smaller than their WT counterpart between E11.5 and E14.5 (Figure 1A). This was associated with a concomitant significant reduction of total FL cellularity (2.4-, 2.2-, and 1.7-fold at E11.5, E12.5, and E14.5, respectively) (Figure 1B). Some but not all E11.5 and E12.5 *Fancg*$^{-/-}$ Pl were also smaller than their WT counterparts, and this reduction in size was always accompanied with a softer structure. Furthermore, overall cellularity of *Fancg*$^{-/-}$ Pl was reduced compared with that of WT Pl (1.3-fold at E11.5 and 1.2-fold at E12.5) (Figure 1B). We next investigated hematopoietic cell content of E12.5 *Fancg*$^{-/-}$ Pl and FL, and E14.5 FL. Fluorescence-activated cell sorting (FACS) analysis markers revealed an important defect of Ter119^{+} erythroid cells both in *Fancg*$^{-/-}$ Pl and FL compared with WT at E12.5 (2- and 8-fold, respectively), and to a significant decrease of GR1^{+} myeloid and B220^{+} lymphoid B cells, but only in the FL (Figure 1C). This overall decrease in hematopoietic lineages in FL was less marked at later stages of development (E14.5, Figure 1C).

Early Defect in Hematopoietic Stem and Progenitor Cells in *Fancg*$^{-/-}$ FL and Pl

We next studied hematopoietic stem and progenitor cell (HSPC)-enriched populations in different sites of hematopoiesis during embryonic development, i.e., AGM, FL, and Pl at E11.5, FL and Pl at E12.5, and FL at E14.5. At

Figure 1. Dysmorphology of *Fancg*$^{-/-}$ Embryos Accompanied with Cellular Defect and Abnormal Hematopoietic Content in the FL and Pl

(A) smaller size and microphthalmia (blue asterisk) of *Fancg*$^{-/-}$ embryos between E11.5 and E14.5, accompanied with a smaller size of FL (red arrowhead). Respective numbers of *Fancg*$^{-/-}$ and WT embryos studied was n = 20 and n = 43 at E11.5, n = 186 and n = 254 at E12.5, and n = 52 and n = 53 at E14.5.

(B) Total cellularity of FL and Pl at E11.5, E12.5, and E14.5.

(C) Total number of erythroid (TER119), myeloid (GR1), and B lymphoid (B220) cells per FL and Pl at E12.5 and E14.5. Black bars, WT; white bars, *Fancg*$^{-/-}$.

Error bars correspond to standard deviation. ***$p < 0.001$, **$p < 0.01$, *$p < 0.05$; NS, not significant.

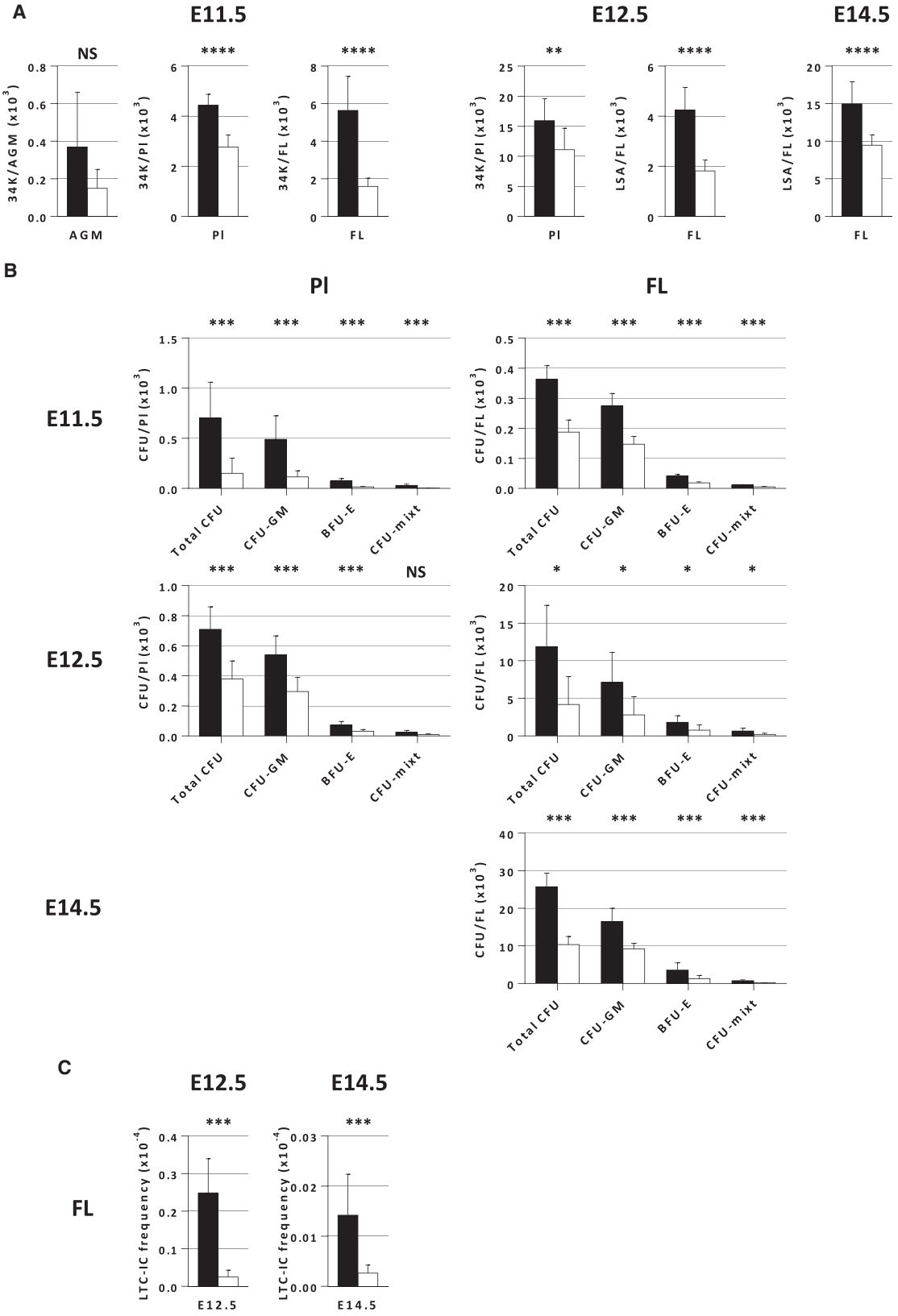

(legend on next page)

E11.5, we chose a $CD34^{+}$c-$KIT^{+/hi}$ (34K) population, which are enriched in HP/HSCs at this early stage of development in the AGM, FL, and Pl (M.S. and L.P., personal communication) (Gekas et al., 2005; Sanchez et al., 1996). These markers were also used for E12.5 PL (Gekas et al., 2005), while for E12.5 and E14.5 FL we used $Lineage^{neg}SCA\text{-}1^{+}AA4.1^{+}$ (LSA) as the reference HSC population (Jordan et al., 1995). At E11.5, we found an overall significant decrease of the 34K population in *Fancg*$^{-/-}$ Pl and FL compared with WT (38% and 72%, respectively), but not in the AGM (Figure 2A). This 34K defect is still present in E12.5 PL (30%). The LSA population was also found to be significantly reduced in E12.5 (57%) and E14.5 FL (37%) (Figure 2A).

Next, we performed *in vitro* functional assays such as clonogenic and long-term culture-initiating cell (LTC-IC) (Petit-Cocault et al., 2007) assays to quantify progenitors and HSPC/HSCs in the FL of *Fancg*$^{-/-}$ embryos at E12.5 and E14.5. As shown on Figure 2B, clonogenic assays revealed that a significant decrease of bipotent colony-forming unit granulocyte macrophage (CFU-GM), burst-forming unit erythroid (BFU-E), and multipotent mixed colony-forming unit (CFU-mixed) was observed at all the stages studied in *Fancg*$^{-/-}$ Pl and FL compared with WT. Collectively, these results uncover a quantitative HP and HSC defect in Pl and FL early during *Fancg*$^{-/-}$ embryonic development, during stages where high HC/HSC amplification takes place.

LTC-IC assays showed that the LTC-IC frequency was 10-fold lower in FL of *Fancg*$^{-/-}$ as compared with WT embryos at E12.5 (Figure 2C). This difference in LTC-IC frequency was less marked in *Fancg*$^{-/-}$ FL at E14.5 (Figure 2C). Altogether these results indicate a severe hematopoietic defect in the immature HP/HSC compartment of *Fancg*$^{-/-}$ FL at E12.5 that gradually attenuates during embryonic development.

Qualitative and Quantitative HSC Defect of *Fancg*$^{-/-}$ FL and Pl at E12.5 Revealed by *In Vivo* Transplantation Assays

To further investigate the HSC compartment at early stages of development in *Fancg*$^{-/-}$ mice, we injected unfractionated FL and Pl cells from E12.5 *Fancg*$^{-/-}$ and WT embryos (CD45.2) into lethally irradiated congenic CD45.1 mice and tested their ability to provide long-term multilineage hematopoietic reconstitution (long-term repopulation [LTR]).

As shown on Figure 3A, when 5×10^5 unfractionated *Fancg*$^{-/-}$ and WT FL cells (which contain the same percentage of 34K and LSA HSC-enriched population [Figure S1] and equivalent to injection of 1,000 *Fancg*$^{-/-}$ or WT LSA) were implanted, only 50% of the recipients injected with *Fancg*$^{-/-}$ FL reconstituted with a low median of blood chimerism (7.1%) while all recipients injected with WT FL reconstituted with a median of engraftment of 70.5%. When 1×10^6 *Fancg*$^{-/-}$ FL cells were injected, 100% of the recipients reconstituted and the median of blood chimerism increased to 57.4%, but remained lower than that of mice injected with the same amount of WT FL cells (79.1%, Figure 3A). This reveals a qualitative defect of E12.5 FL *Fancg*$^{-/-}$ HSCs. This HSC defect is even more important in the Pl, since primary recipients barely reconstituted when 5×10^5 or 1×10^6 unfractionated E12.5 *Fancg*$^{-/-}$ Pl cells were injected (median of blood chimerism of 5% and 9.1%, respectively, versus 91.7% for mice injected with 5×10^5 WT Pl cells) (Figure 3B).

Twenty to 24 weeks post injection, extensive FACS analysis of reconstituted recipient BM for co-expression of CD45.2 and specific lineage markers indicated that HSCs from FL and Pl of *Fancg*$^{-/-}$ mice were able to give rise to all hematopoietic lineages in adult recipients, although less efficiently than WT FL or Pl, especially for GR1 myeloid lineage, and to a lesser extent for B220 B lymphoid lineage (Figures 3C and 3D, respectively). This suggests a loss of myeloid potential of E12.5 *Fancg*$^{-/-}$ FL and Pl HSCs at this stage. No secondary reconstitution was observed with 5×10^5 unfractionated BM cells from primary recipients injected with *Fancg*$^{-/-}$ FL or Pl, even when BM cells injected presented a high CD45.2 chimerism (79.6%), while all mice injected with BM cells from primary recipients injected with WT FL or Pl reconstituted (Table 1). Taken together, these results suggest that early during development, when high HC/HSC amplification takes place in FL and Pl, there is an impairment of proliferative and self-renewal capacities of HSCs in *Fancg*$^{-/-}$ FL and Pl, along with an important loss of all hematopoietic lineages potential, especially myeloid.

This HSC qualitative defect persists in *Fancg*$^{-/-}$ FL at E14.5, as described by others for *Fancc*$^{-/-}$ and *Fancd2*$^{-/-}$

Figure 2. Defect of HSPC-Enriched Populations and CFUs in the Pl and FL of *Fancg*$^{-/-}$ Embryos Is Observed as Soon as E11.5

(A) Total number of HSPC-enriched cells in the Pl and FL at E11.5 and E12.5, and in the FL at E14.5. At E11.5 in the AGM (n = 4), Pl (n = 3), and FL (n = 3), and at E12.5 in the Pl (n = 9) the HSPC-enriched population is 34K, while in the FL at E12.5 (n = 7) and E14.5 (n = 6) it is LSA. (B) Total CFUs and CFU-GM, BFU-E, and CFU-mixed content per FL at E11.5, E12.5, and E14.5 and per Pl at E11.5 and E12.5. Results shown represent the mean ± SE and correspond to 3–5 independent experiments, with two independent Petri dishes scored for each experiment. (C) *In vitro* comparison of LTC-IC frequency in *Fancg*$^{-/-}$ and WT FL at E12.5 (n = 3) and E14.5 (n = 3). n represents distinct experiments. Error bars correspond to standard deviation. Black bars, WT; white bars, *Fancg*$^{-/-}$. **** p<0.0001, ***p < 0.001, **p < 0.01, *p < 0.05; NS, not significant.

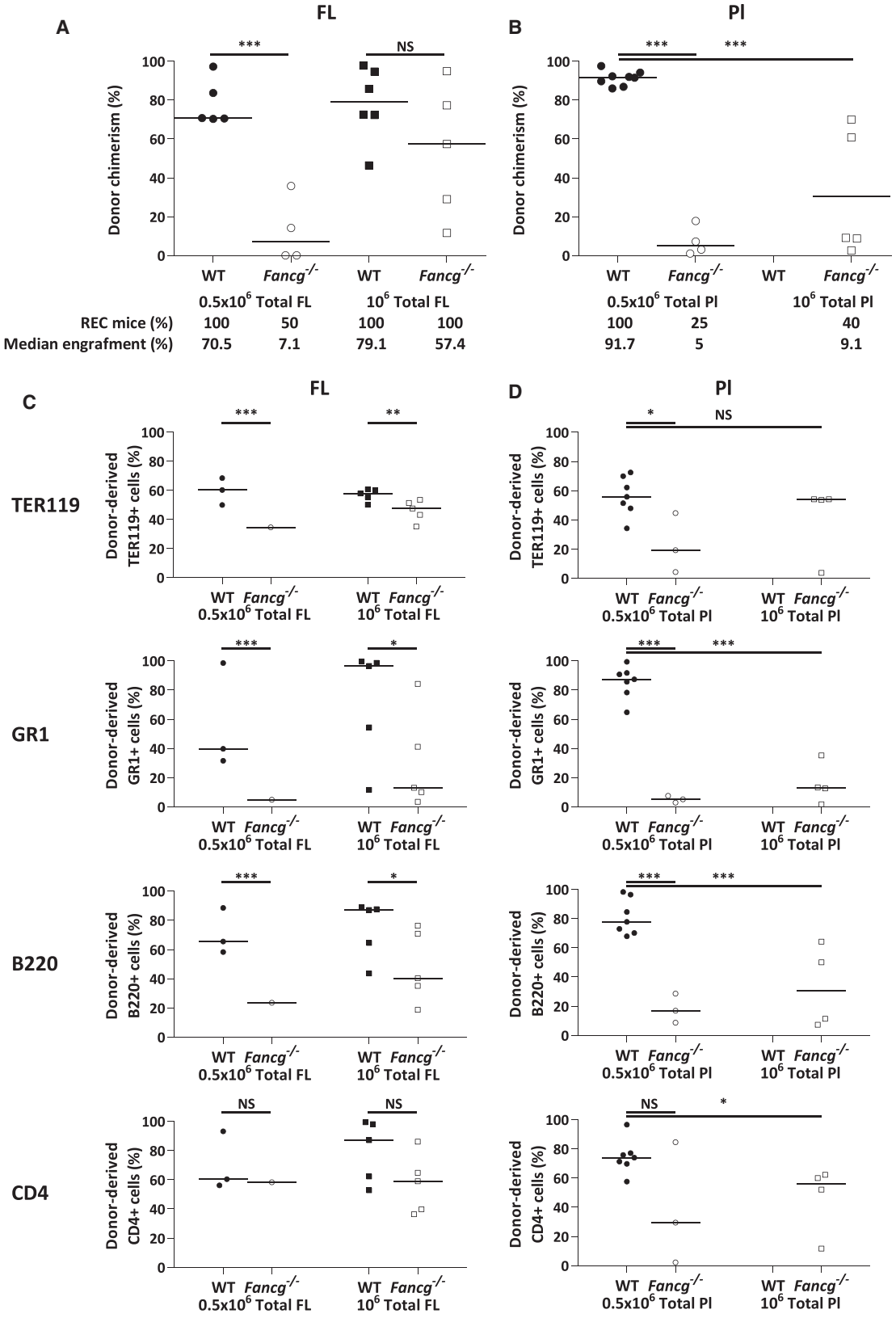

(legend on next page)

Table 1. Secondary Reconstitutions with BM from Primary Recipients Injected with *Fancg*$^{-/-}$ and WT Pl and FL

Primary Transplantation		Secondary Transplantation: No. of BM Cells Injected	Engrafted Mice[a]/ Total Mice	Median Reconstitution (%) [Lower Rec – Higher Rec]
E12.5 PL	WT	5×10^5	5/5	11.6 [6.3 – 25.5]
	Fancg$^{-/-}$	5×10^5	0/5	0.07 [0 – 2]
E12.5 FL	WT	5×10^5	3/3	15.9 [9.3 – 18.6]
	Fancg$^{-/-}$	5×10^5	0/6	1.7 [0.5 – 3.6]

[a]Engraftment was considered as positive when CD45.2 chimerism in the blood was >5%.

(Kamimae-Lanning et al., 2013; Suzuki et al., 2017; Yoon et al., 2016). An HSC-enriched LSA population sorted from *Fancg*$^{-/-}$ and WT E14.5 FL was injected into lethally irradiated primary CD45.1 mice. Twenty weeks post injection, median blood chimerism was only 20.5% when 1,000 *Fancg*$^{-/-}$ LSA cells were injected, compared with 86.8% for 1,000 WT LSA cells (Figure S2A). When 5,000 LSA *Fancg*$^{-/-}$ cells were injected, high blood chimerism ($\geq$70%) was observed in 50% of the mice (Figure S2A). However, an overall important defect in the GR1 myeloid lineage in the BM was still observed (Figure S2B), as well as a low level of blood chimerism when secondary transplantations were performed (Figure S2C), which indicates that at E14.5 *Fancg*$^{-/-}$ LSA HSCs are still defective for proliferation, self-renewal, and myeloid differentiation. Collectively, these analyses highlight a compromised function of *Fancg*$^{-/-}$ HSCs during embryonic development, which is more important at early stages when hematopoietic amplification peaks.

No Cell-Cycle Changes or Increased Apoptosis but Mild Increase of DNA Damage in E12.5 *Fancg*$^{-/-}$ FL HSCs

Given the high level of amplification of HSCs occurring at early stages of embryonic development, we investigated whether there was an increase in DNA damage as assessed by evaluation of γH2AX level in various E12.5 Pl and FL, and E14.5 FL populations (fractionated and unfractionated) from *Fancg*$^{-/-}$ and WT by flow cytometry. At E12.5, no difference in γH2AX level (mean fluorescence intensity [MFI]) was observed between E12.5 *Fancg*$^{-/-}$ and WT HCs (CD45) and HSCs (34K) in Pl, while in FL, although overall not statistically significant, higher levels of γH2AX were found in all *Fancg*$^{-/-}$ hematopoietic populations compared with WT for each individual experiment performed, especially in the HSC-enriched LSA population (Figure 4A). This increase in γH2AX-positive cells was no longer observed in all hematopoietic populations tested at E14.5 in *Fancg*$^{-/-}$ FL (Figure 4A). No increase in apoptosis was observed in the E12.5 FL LSA population (Figure S3A).

G_0, G_1, S, and G_2/M phases of cell cycle were analyzed by flow cytometry in *Fancg*$^{-/-}$ and WT HSCs using Hoechst 33,342/pyronine staining. At E12.5, no significant difference for any of the cell-cycle phases was observed between *Fancg*$^{-/-}$ and WT HCs or HSCs populations in FL or Pl, except an increase in G_0 for 34K Pl HSCs ($p < 0.05$) (Figure 4B). In E14.5 *Fancg*$^{-/-}$ FL, there was an increase in G_1 phase for CD45 HCs and LSA HSCs ($p < 0.05$) compared with WT FL, and a decrease in S phase for CD45 HCs (Figure 4B).

HSPC Defect in the FL of Human FA Embryo

We could obtain FL samples from six human fetuses after medical abortion, strongly suspected, based on malformative signs, to have FA. Among the six, one fetus (13 weeks of gestation [WG]) was subsequently confirmed as FA and specifically diagnosed *FANCB*, while FA was ruled out in the others. FANCB is part of the FA core complex, as FANCG, and it has been recently shown in mouse that *Fancb* deficiency impairs HSC function (Du et al., 2015). We isolated a $CD34^+CD38^-CD45^+CD117(cKIT)^{hi}$ cell population in normal human FL, which presents typical functional and molecular features of HSCs (L.M. et al., unpublished data). We therefore used this combination of markers to sort HSCs from the FA FL and from two normal FL of matched stages of development (13 and 17.7 WG). As shown in Figure 5A, the $CD34^+CD38^-CD45^+CD117^{hi}$ population is 55-fold less frequent in FA FL than in control FL (0.0017 versus 0.093%). *In vitro* LTC-IC assays revealed a

Figure 3. High LTR Ability Defect and Impaired Myeloid Potential in E12.5 *Fancg*$^{-/-}$ Pl and FL

(A) CD45.2 chimerism in the blood of primary recipients 20–24 weeks post injection of 5×10^5 (circles) or 10^6 (squares) WT (black) or *Fancg*$^{-/-}$ (white) total FL cells.

(B) CD45.2 chimerism in primary recipients' blood 20–24 weeks post injection of 5×10^5 (circles) or 10^6 (squares) WT (black) or *Fancg*$^{-/-}$ (white) Pl cells.

(C and D) Analysis of BM hematopoietic content of primary recipients transplanted with FL (C) or Pl (D), expressed as a percentage of $CD45.2^+$ erythroid (TER119), myeloid (GR1), B lymphoid (B220), and T-lymphoid (CD4) cells. Circles, 5×10^5 cells injected; squares, 1×10^6 cells injected; black, WT FL or Pl cells; white, *Fancg*$^{-/-}$ FL or Pl cells.

***$p < 0.001$, **$p < 0.01$, *$p < 0.05$; NS, not significant.

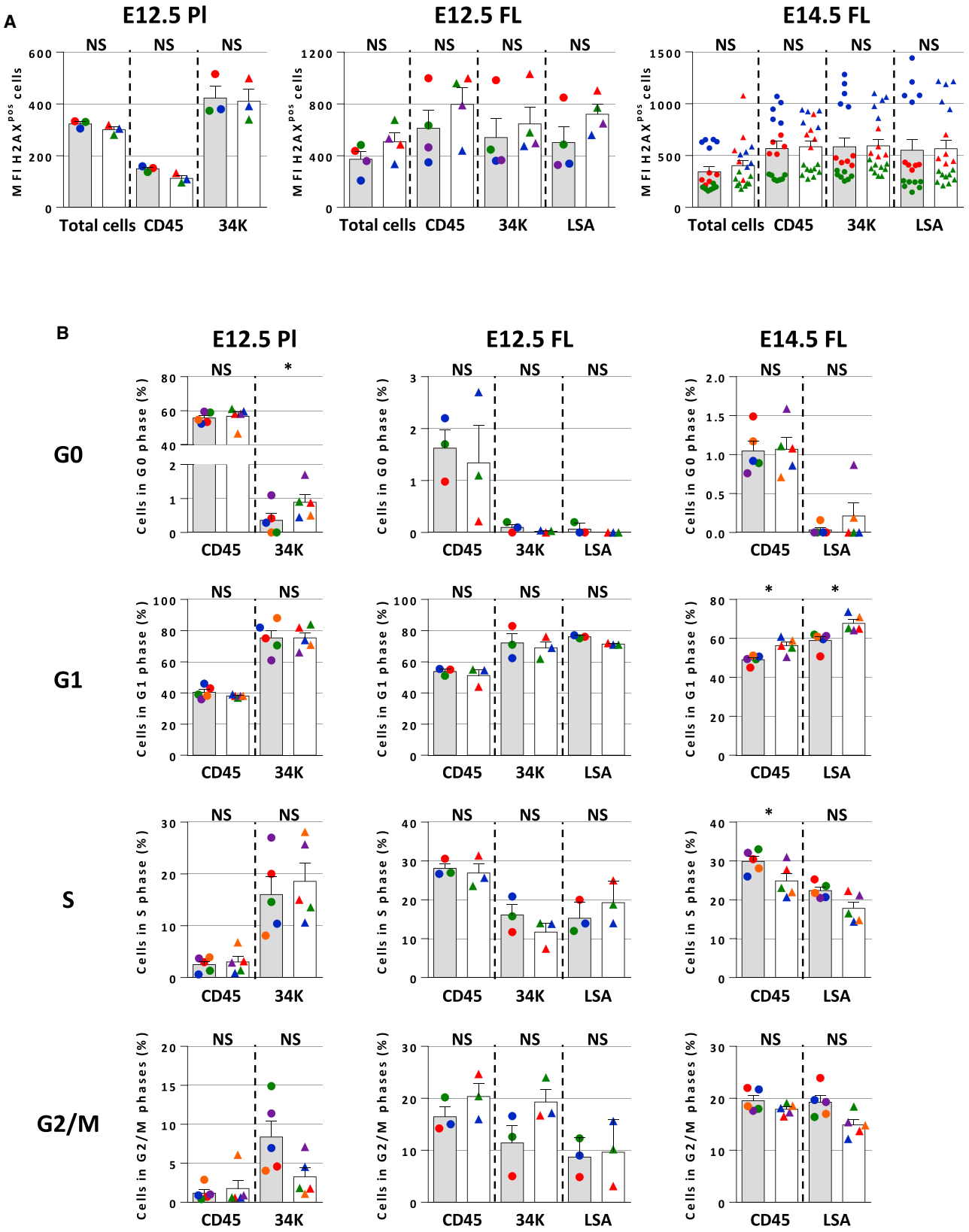

(legend on next page)

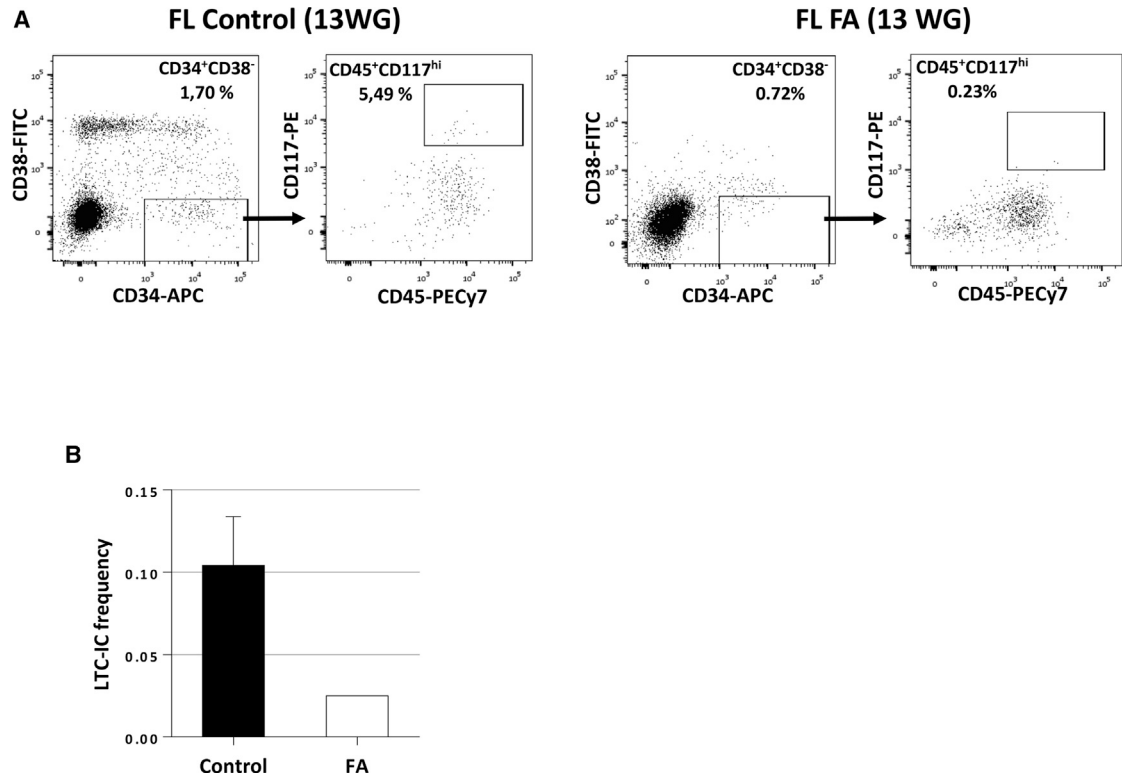

Figure 5. Important Frequency and LTC-IC Defect in the CD34$^+$CD38$^-$CD45$^+$CD117^{hi} HSC-Enriched Population of a Human FA 13 WG FL

(A) Comparison of the frequency of CD34$^+$CD38$^-$CD45$^+$CD117^{hi} HSC-enriched population from an FA (*FANCB*) FL or from an age-matched control FL (13 WG).

(B) Comparison of LTC-IC frequency of CD34$^+$CD38$^-$CD45$^+$CD117^{hi} cells sorted from an FA (*FANCB*) FL (13 WG) and from two age-matched control FL (13 and 17.7 WG).

Error bars correspond to standard deviation. Black bar, control FL; white bar, FA FL.

3.9-fold lower frequency of LTC-IC in the CD34$^+$CD38$^-$CD45$^+$CD117^{hi} HSC-enriched population sorted from the FA FL as compared with the same population sorted from the two control FLs (Figure 5B). In addition, we were unable to amplify FA CD34$^+$CD38$^-$CD45$^+$CD117^{hi} LTC-ICs when reseeded on fresh MS5 (extended LTC-IC), while CD34$^+$CD38$^-$CD45$^+$CD117^{hi} LTC-ICs issued from a normal FL of 15 WG and cultured in the same conditions could be amplified for more than 6 months (from 10^2 HCs to 10^{14}, L.M. et al., unpublished data). These data demonstrate that a hematopoietic deficit is also already present during embryonic hematopoietic development in a human FA fetus.

Similar Transcriptome Profiles of E12.5 *Fancg*$^{-/-}$ and Human FA FL HSCs and Identification of Compensatory Transcriptomic Regulation in E14.5 *Fancg*$^{-/-}$ FL

To identify signaling pathways or gene regulatory networks deregulated in mouse *Fancg*$^{-/-}$ and in human FA HSCs, we performed gene expression analysis and compared *Fancg*$^{-/-}$ and WT HSCs sorted from mouse FL at E12.5 and E14.5, but also FA and normal HSCs sorted from human FL.

Mouse FL LSA HSC-enriched populations were sorted in three independent experiments. A total of 11,071 genes were found to be differentially expressed between *Fancg*$^{-/-}$

Figure 4. Induced DNA Damage in E12.5 and E14.5 *Fancg*$^{-/-}$ HCs and HSCs without Apoptosis or Cell-Cycle Changes

(A) MFI of γH2AX^{pos} cells in total, HC (CD45), and HSC (34K or SA) in E12.5 PL (n = 3), FL (n = 4), and E14.5 FL (n = 3, and each dot represents an individual mouse), measured by flow cytometry.

(B) Histograms of G_0, G_1, S, and G_2/M phases of the cell cycle determined after Hoechst staining, for *Fancg*$^{-/-}$ and WT HC, and HSCs of E12.5 FL and Pl and E14.5 FL. Dots of same colors are related to the same experiment.

Error bars correspond to standard deviation. Gray bars, WT; white bars, *Fancg*$^{-/-}$. *p < 0.05; NS, not significant.

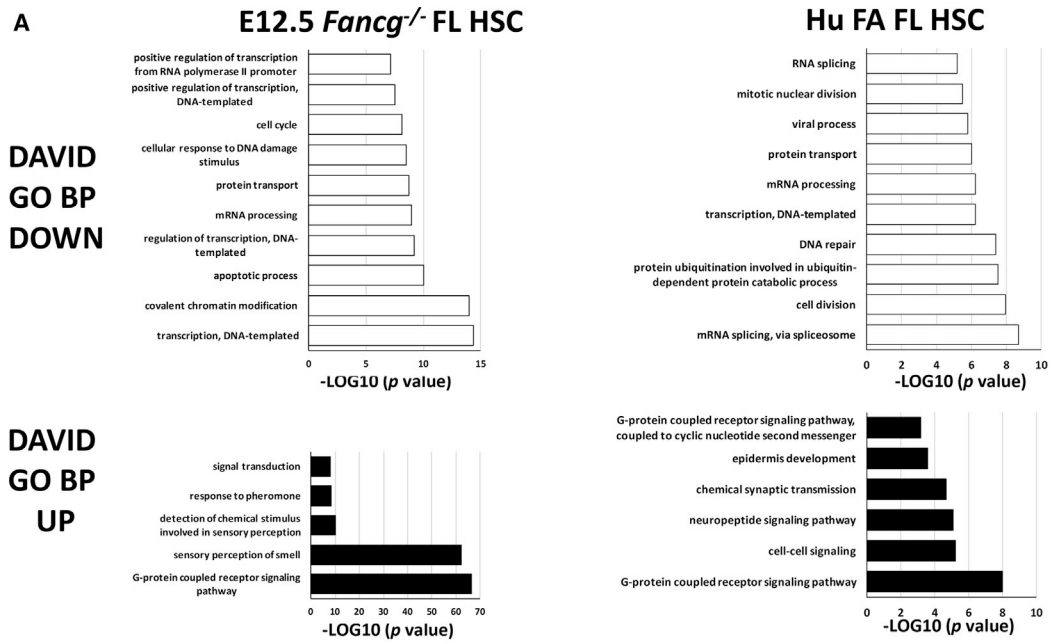

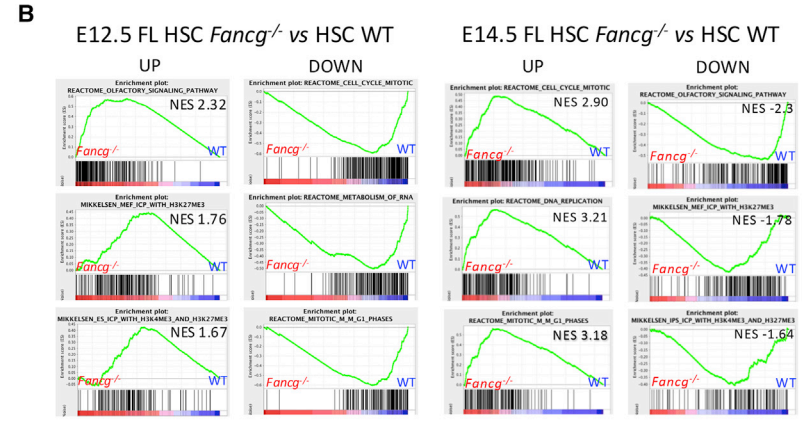

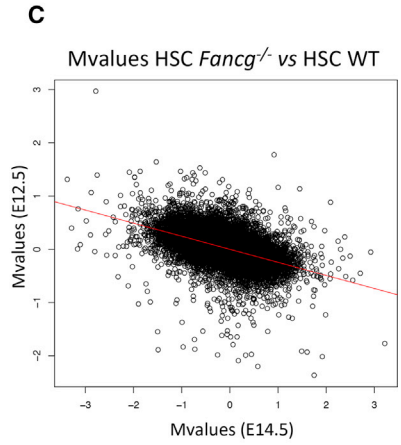

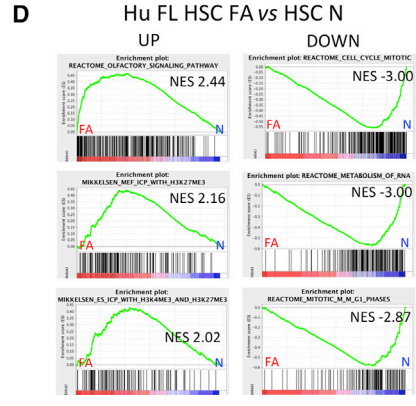

(legend on next page)

and WT HSCs in E12.5 FL (one-way ANOVA, $p < 0.05$), with 4,033 upregulated and 2,024 downregulated in *Fancg*$^{-/-}$ (fold change [FC] >1.5 or < −1.5). Gene ontology (GO) analysis indicated that the main biological processes (BP) downregulated in *Fancg*$^{-/-}$ FL HSCs at E12.5 were involved in transcription process, cell cycle, covalent chromatin modification, and DNA repair (Figure 6A and Table S1). Strikingly, for upregulated genes BP were associated with sensory perception of smell and GPCR signaling pathway (Figure 6A and Table S1). At E14.5, only 561 genes were differentially expressed ($p < 0.05$), with 166 upregulated and 82 downregulated in *Fancg*$^{-/-}$ (FC >1.5 or < −1.5), indicating that at this stage differences in gene expression between *Fancg*$^{-/-}$ and WT HSCs are fading. No significant BP was found for downregulated genes, and for upregulated genes the main BPs were related to angiogenesis, cell migration, and hypoxia (Table S1). Gene set enrichment analysis (GSEA) confirmed that genes upregulated in E12.5 FL *Fancg*$^{-/-}$ HSCs were most enriched in the "reactome olfactory signaling pathway," but also in H3K4 and H3K27 trimethylation (H3K4Me3 and H3K27Me3) pathways (Figure 6B), which allows discriminating genes that are expressed, repressed, or poised for expression (Mikkelsen et al., 2007). It also supported the fact that genes downregulated are most enriched in cell cycle and metabolism of RNA reactomes (Figure 6B). Interestingly, GSEA analysis of E14.5 FL *Fancg*$^{-/-}$ HSC transcriptome revealed the exact opposite situation, i.e., that *Fancg*$^{-/-}$ LSA upregulated genes are most enriched in cell cycle and RNA metabolism, while downregulated genes are most enriched in "reactome olfactory signaling pathway" and in both H3K4 and H3K27 trimethylation (H3K4Me3 and H3K27Me3) pathways, as if at E14.5 a compensatory transcriptome regulation is accompanying the phenotypical and functional compensation that we describe. An anticorrelation study between *Fancg*$^{-/-}$ and WT HSCs at E12.5 against E14.5 shows an inversion of FC (Pearson correlation coefficient between M values [or log2(FC)] between E12.5 and E14.5 is −0.6). This result supports this compensation at E14.5 (Figure 6C).

We also achieved human transcriptome on sorted $CD34^{+}CD38^{-}CD45^{+}CD117^{hi}$ HSC-enriched population from the unique FA FL (13 WG), and from two normal FLs from fetuses at the same stage of development (i.e., second trimester, 13 and 17.7 WG). Transcriptome analysis showed that 5,806 genes were differentially expressed between FA and normal FL HSCs (one-way ANOVA, $p < 0.05$), with 3,156 genes upregulated and 1,631 downregulated in FA FL. GO analysis indicated that as for E12.5 *Fancg*$^{-/-}$ FL CSHs, the main BP downregulated were also involved in the transcription process, cell cycle, and cell division, while the GPCR signaling pathway was the most significant upregulated BP, GSEA supporting that upregulated genes were most enriched in the "reactome olfactory signaling pathway" (162 out of 297 genes) (Figures 6A and 6D; Table S1).

Regarding a short list of genes involved in cell-cycle control, we found a dysregulation of these genes in E12.5 FL *Fancg*$^{-/-}$ HSCs and FA FL HSCs, with downregulation of both positive (*CDK1*, *CDK6*, *CDC7*, *CDKN3*) and negative (*P16*, *P19*) regulators of cell cycle (Table S2). This dysregulation is no longer observed at E14.5, and only *CDKN1A* (p21) is significantly upregulated (Table S2). This upregulation is also observed in FA HSCs, as described by Ceccaldi et al. (2012) for whole FA fetal liver samples. *p53* gene is also significantly downregulated in E12.5 *Fancg*$^{-/-}$ FL HSCs and in human FA FL HSCs (Table S2), which was confirmed by qRT-PCR (Figure S3B). Analyses of phosphorylated p53 expression by flow cytometry did not reveal any significant difference between *Fancg*$^{-/-}$ and WT E12.5 FL HCs or HSPCs (Figure S3C).

We also investigated transcriptional regulators and markers described as being important for HSC development and maintenance. As shown on Table S3, most of these genes were significantly and highly decreased in FL *Fancg*$^{-/-}$ HSCs at E12.5, while no significant change was detected at E14.5. Decrease of *Hlf*, *Flt3*, and *Mll1* in E12.5 FL *Fancg*$^{-/-}$ HSCs was confirmed by qRT-PCR (Figure S3D). Decreased expression of transcriptional regulators and markers important for HSCs was also observed in human FA FL HSCs, although to a lesser extent (Table S3).

Altogether our analysis indicates that HSCs isolated from a second trimester human *FANCB* FL present a transcriptomic profile very close to E12.5 *Fancg*$^{-/-}$ FL HSCs.

DISCUSSION

In the present paper, using a *Fancg*$^{-/-}$ mouse model of FA we show that HSC defect starts very early during

Figure 6. Highly Conserved GO Biological Processes between E12.5 *Fancg*$^{-/-}$ Pl and FL and Human FA FL HSCs

(A) Enriched GO biological process (BP) terms for downregulated (white bars) and upregulated (black bars) genes in E12.5 *Fancg*$^{-/-}$ FL HSCs and in human FA FL HSCs. GO BPs determined using DAVID annotation tool are expressed as $-\log_{10}$ (p value). NES, normalized enrichment score.

(B) GSEA plots for up- and downregulated genes, specifically expressed in E12.5 and E14.5 Fancg$^{-/-}$ FL HSCs.

(C) Anticorrelation study. Plot of $\log_2$(FC) between *Fancg*$^{-/-}$ and WT HSCs at E12.5 against E14.5.

(D) GSEA plots for up- and downregulated genes, specifically expressed in human FA FL HSCs.

embryogenesis, during the earliest steps of hematopoietic amplification in FL and Pl. We also show that an HSC defect is also observed in the FL of a human FA (*FANCB*) fetus.

The hypothesis that FA BMF could take its origin *in utero* was suggested by the study of Ceccaldi et al. (2012) and was corroborated by studies of fetal hematopoiesis in E14.5 *Fancc*$^{-/-}$ and *Fancd2*$^{-/-}$ FL (Kamimae-Lanning et al., 2013; Suzuki et al., 2017; Yoon et al., 2016). In the present work, we followed hematopoiesis in *Fancg*$^{-/-}$ mice using state-of-the-art experimental hematopoiesis assays including long-term engraftment experiments on highly purified mouse and human cells. In an original way compared with previous studies, we focused on a crucial developmental window that spans from the onset of hematopoiesis in the AGM region at E11.5 until late HSC amplification in E14.5 FL, and also studied the Pl, which has been shown to be an important reservoir of HSCs during mouse development (Gekas et al., 2010; Ottersbach and Dzierzak, 2010). We paid particular attention to E12.5 when amplification peaks, both in Pl and FL (Medvinsky et al., 2011). Our study demonstrates that HSC impairment starts both in FL and Pl early during mouse development at E11.5, and is still present at E12.5 in these organs. *In vivo* transplantations revealed important quantitative and qualitative defect of *Fancg*$^{-/-}$ E12.5 FL and Pl HSCs, and pointed out an exhaustion in their proliferative and self-renewal capacities, with a loss of hematopoietic lineage potential, especially myeloid. This applies also to *Fancg*$^{-/-}$ FL LSA HSCs at E14.5, but to a lesser extent. Between E11.5 and E14.5 in the FL and between E11.5 and E12.5 in the Pl, HSCs are rapidly cycling, and therefore under high DNA replication stress, which could explain their compromised function in the *Fancg*$^{-/-}$ context. Actually, although not significant, an elevation of γH2AX in the hematopoietic populations (especially HSCs) studied by flow cytometry was observed in E12.5 *Fancg*$^{-/-}$ FL, indicative of a replication stress at this stage. Nevertheless, no increase in apoptosis, nor cell-cycle change, could be observed. Elevation of γH2AX was no longer detected in E14.5 FL.

All these observations indicate that during *Fancg*$^{-/-}$ embryonic development, HSC deficit is worse at E12.5 than at E14.5. Of note, external phenotypic signs of Fanconi disease such as smaller size, microphthalmia, or anophthalmia are also more pronounced early during development (E11.5–E12.5) and tend to attenuate around E14.5 (Figure 1). Indeed, as development progresses, phenotypic features of *Fancg*$^{-/-}$ embryos are more heterogeneous, some of them looking almost like WT embryos, including FL size (data not shown). Likewise, transcriptomic analysis also showed that in contrast to E12.5 FL, very few genes were significantly differentially expressed in E14.5 FL between *Fancg*$^{-/-}$ and WT HSCs. One possible explanation is that *Fancg*$^{-/-}$ embryos that are more deeply affected die around E14.5 (which could also explain the collapsed frequency of *Fancg*$^{-/-}$ mice at birth) and that a compensatory amplification takes place when proliferative stress decreases, making transcriptomic differences between *Fancg*$^{-/-}$ and WT HSCs less important, although functional defect remains. Actually, GSEA analysis of the transcriptome of E12.5 and E14.5 *Fancg*$^{-/-}$ and WT FL HSCs is in agreement with a compensatory molecular regulation at E14.5, since BP downregulated at E12.5 are upregulated at E14.5, and vice versa (Figure 6B).

Importantly, we also show that HSC function is also already impaired *in utero* in humans. During human development HSC amplification takes place in the FL, during the first and part of the second trimester. Our analysis of HSC-enriched CD34^{+}CD38^{-}CD45^{+}CD117^{hi} population from a 13 WG *FANCB* FL revealed both an important decrease in the frequency (55-fold) and functional activity (LTC-IC frequency) (4-fold) of this population compared with normal FL of matched stages of development.

Interestingly, transcriptomic analysis showed that differentially up- and downregulated genes in HSCs from human FA were found to be involved in the very same BP as in HSCs from E12.5 *Fancg*$^{-/-}$ FL, i.e., cell division, cell cycle, mRNA processing, and covalent chromatin modification for downregulated genes and GPCR pathway and olfactory signaling pathway for upregulated genes. This indicates that pathways dysregulated in fetal FA HSCs seem to be highly conserved between mouse and human during development.

Most of the genes involved in cell-cycle regulation are downregulated in *Fancg*$^{-/-}$ E12.5 FL, whether they are positive or negative regulators (Table S2). This dysregulation is also observed in human FA FL HSCs (Table S2). In line with the results described for *Fancd2*$^{-/-}$ E14.5 FL HSCs (Suzuki et al., 2017; Yoon et al., 2016), *p53* gene is significantly downregulated both in *Fancg*$^{-/-}$ and FA fetal HSCs. In a genotoxic stress model, Milyavsky et al. (2010) showed that upon serial transplantations, HSCs submitted to γ-irradiation with disabled p53 accumulated DNA damage and exhibited decreased self-renewal capacity. In the same way, during the replicative stress that occurs in the FL during embryonic development, the decrease in p53 signaling pathway in HSCs could lead to the defect in self-renewal that we observed during secondary transplants of BM from primary recipients injected with *Fancg*$^{-/-}$ FL or Pl, even when BM cells injected presented a high CD45.2 chimerism.

GSEA analysis also uncovered epigenetic dysregulations of E12.5 *Fancg*$^{-/-}$ and human FA FL HSCs (Figures 6B and 6D), which could play an important role during the phases of high cell division and DNA replication that take place during embryogenesis. Epigenetic control is important to preserve normal homeostasis by regulating stem cell

self-renewal versus differentiation in multiple tissue-specific stem cells (Beerman and Rossi, 2015). An aberrant epigenetic control of gene expression-maintaining HSC compartment has been recently hypothesized to explain defective FA hematopoiesis (Brosh et al., 2017), and our results during embryonic development are in line with this proposition.

GPCR and olfactory signaling pathways were the main BP covering upregulated genes in *Fancg*$^{-/-}$ and FA FL HSCs. Actually GPCRs contribute to hematopoietic regulation, these receptors being the direct link between HSCs and their microenvironment that hosts many hematopoietic regulators and neurotrophic factors (Ramkissoon et al., 2006). The importance of the sympathetic system has been underlined not only for maintaining homeostasis of adult BM (Mendelson and Frenette, 2014), but also in emergence of HSCs in mouse AGM (Fitch et al., 2012). A recent report also demonstrates an olfactory control of blood progenitor maintenance in *Drosophila* (Shim et al., 2013).

Our unique kinetics study reveals that a deep HSCs defect is already present very early during *Fancg*$^{-/-}$ mouse development, and that FA clinical and biological manifestations are more severe at early times of development (E11.5–E12.5), and are mitigated at E14.5. A deep HSC defect is also observed during human FA development, and human FA FL HSCs present a transcriptome profile similar to that of mouse E12.5 *Fancg*$^{-/-}$ FL HSCs. Our model sheds light on the interest of positioning the study of *Fanc* knockout hematopoiesis earlier than E14.5, during the steps of highest HSC/HC amplification in the mouse embryo. Indeed, despite the fact that FL failure seems to go through different mechanisms than adult BM failure, it might represent a good alternative model to study hematopoietic failure and certainly presents important potential clinical relevance.

EXPERIMENTAL PROCEDURES

Fancg$^{-/-}$ Embryos

Fancg$^{-/-}$ mice (Koomen et al., 2002) were back-crossed on C57Bl6 background (n = 8). *Fancg*$^{-/-}$ and WT embryos were produced by natural mating of C57Bl6/J *Fancg* heterozygote mice. Vaginal plugs were checked in the morning, marking E0.5. The stages of the embryos used were confirmed by somite counting and/or morphological analysis. Embryos were dissected further to recover placenta and liver. Embryo tails were genotyped using the Phire PCR Kit (Thermo Scientific). All animal procedures reported in this paper were carried out in accordance with French Government regulations (Services Vétérinaires de la Santé et de la Production Animale, Ministère de l'Agriculture).

Human Fanconi Embryo

Control FL samples, as well as FL used for medical diagnosis of FA after termination of birth, were obtained from therapeutic abortions, with informed consent of the family. This was in compliance with French laws, and with a specific authorization of the French Biomedicine Agency for this project.

Cell Preparation

Single-cell suspensions of FL were prepared in DMEM medium (Fischer) with 10% fetal calf serum (FCS) (Eurobio) by repeated flushing through 23- to 26-gauge needles. Placentas were dissected and treated for 1 hr at 37°C with type I collagenase (Sigma) (0.125% in PBS with 10% FCS). After washing, cell suspension was filtered through 70-μm nylon mesh and resuspended in DMEM supplemented with 10% FCS.

Clonogenic Assays

Methylcellulose progenitor assays were performed as previously described (Petit-Cocault et al., 2007): 5×10^4 FL or 1×10^5 PL cells were plated in 1 mL of 0.8% methylcellulose in IMDM supplemented with 30% FCS, 1% BSA (Sigma), and 10^{-4} M β-mercaptoethanol (Sigma), in the presence of 2 U/mL erythropoietin, 10 ng/mL mouse interleukin-3, 50 ng/mL stem cell factor, and 20 ng/mL human thrombopoietin (Promocell). Samples were plated in duplicate 35-mm Petri dishes and the number of total colonies was scored after an incubation of 7 days at 37°C and 5% CO_2.

Long-Term Culture-Initiating Cells Assay

LTC-IC assay was performed as previously described (Petit-Cocault et al., 2007). In brief, 3×10^3 MS5 stromal cells (Itoh et al., 1989) were seeded in LTC-IC medium in 96-well flat-bottom microplates and serial half-dilutions of test cells seeded over 24 hr later. Cultures were maintained at 37°C, 5% CO_2 with weekly half-medium changes. Presence of cobblestone area forming colony (CAF-C) after 4 (mouse) or 5 (human) weeks of culture was quantified. Frequency of LTC-ICs was determined using L-Calc software (STEMCELL Technologies).

Analysis of Long-Term Repopulating Ability

Adult C57Bl6/Ly5.1 mice were lethally irradiated (9.5 Gy), and *Fancg*$^{-/-}$ or WT E12.5 total FL or Pl (C57Bl6/Ly5.2) were injected intravenously into the retro-orbital venous plexus. For E14.5 FL, lineage^{neg}SCA-1$^+$AA4.1$^+$ (LSA) sorted cells were co-injected with 5×10^5 C57Bl6/Ly5.1 spleen cells for short-term radioprotection. Peripheral blood was collected at different times after injection and nucleated cells were incubated with CD45-LY5.1 (CD45.1) APC-conjugated and CD45-LY5.2 (CD45.2) PE-conjugated (Biolegend, BLE110714 and BLE109808), and analyzed by flow cytometry for the presence of donor-derived (LY5.2$^+$) cells. The percentage of reconstitution was determined as follows: (%LY5.2/%LY5.1 + %LY5.2) × 100. A recipient mouse was considered positive when the percentage of reconstitution was above 10% for primary reconstitutions and 5% for secondary reconstitutions.

Multilineage Analysis and Secondary Transplantation

Primary recipient mice were sacrificed 20–24 weeks after primary transplant, and BM content was analyzed by flow cytometry after incubation with CD45.2 (PE), c-KIT (PE-Cy7), and APC-conjugated SCA-1, TER119, CD71, GR1, CD11B, CD41, CD61, CD19, B220,

CD4, or CD8 (PE-Cy7) antibodies (Biolegend, BLE109808, BLE105814, and BLE108112; BLE116211, BLE113820, BLE108412, BLE101212, BLE133914, BLE104316, BLE115512, BLE103211, BLE100412, or BLE100722) (Petit-Cocault et al., 2007). The percentage of co-expression of CD45.2 and lineage markers was determined using the software FlowJo 10.1 (TreeStar). At the same time, 5×10^5 BM cells from primary mice transplanted with *Fancg*$^{-/-}$ and WT samples were injected into new C57Bl6/Ly5.1 irradiated mice for secondary reconstitution. Mice were bled 7–10 weeks after injection to determine the percentage of reconstitution.

Cytometry Analysis and Cell Sorting

Murine FL cells were depleted of lineage-positive cells using MACs Micro Beads (Miltenyi Biotec) with a mixture of TER119, GR1, B220, CD4. and CD8a monoclonal antibodies (Biolegend, BLE116202, BLE108402, BLE103202, BLE100402, and BLE100702). This lineage^{neg} fraction was incubated with SCA-1 (APC) and AA4.1 (PE) antibodies (Biolegend, BLE108112 and BLE136504) and SCA-1$^+$AA4.1$^+$ cells (LSA) sorted on a FACSAria SORT cell sorter (BD Biosciences). Human FL cells were sorted after incubation with CD34 (APC), CD38 (FITC), CD45 (PE-Cy7) and CD117 (PE) antibodies (Biolegend, BLE343510, BLE303504, BLE304016 and BLE313204). DAPI (4′,6-diamidino-2-phenylindole) was used to exclude dead cells. For Pl, HSC CD34$^+$c-KIT^{hi} population was sorted without lineage depletion (Biolegend, BLE343506 and BLE313212).

Cytometric analysis for FL and Pl cells used similar antibodies as for LTR studies and sorted cells, with an exclusion of dead cells by DAPI. Data were collected on LSRII (BD Biosciences) or MACSQuant analyzer 10 (Miltenyi), and analyzed using FlowJo 10.1 (TreeStar).

Cell Cycle and Apoptosis

Cell-cycle analysis was performed on E12.5 FL and Pl and E14.5 FL HC and HSC populations with Hoechst 33,342 staining protocol (Kim and Sederstrom, 2015). Cells were suspended at a concentration of 1×10^6/mL in pre-warmed medium, and Hoechst was added to a final concentration of 5 μg/mL. After incubation at 37°C for 45 min, Pyronin Y was added to a final concentration of 0.4 μg/mL and the cells were incubated at 37°C for 15 min. Cold PBS was added before incubation at +4°C with antibodies. Dead cells were excluded with 7-AAD and samples were run on a FACS-FORTESSA cytometer (BD Biosciences).

For apoptosis, immunostained cells were suspended in Annexin V buffer and stained with FITC-Annexin V (Biolegend, BLE640905) and DAPI, according to the manufacturer's guidelines. FACS analysis was performed on a FACSCanto analyzer (BD Biosciences).

DNA Damage-Induced Phosphorylation of H2AX (γH2AX) and Analysis of p53 Phosphorylation

Replicative stress induces DNA damage, which induces phosphorylation of the histone H2AX variant to γH2AX (Greve et al., 2012). E12.5 FL cells were incubated with CD45 or CD34, c-KIT, SCA-1, and AA4.1 antibodies, fixed with paraformaldehyde 4% at +4°C, washed and permeabilized in 0.25% Triton X-100, and incubated with monoclonal anti-phosphate Histone H2AX (Ser139) antibody (clone N1-431) conjugated to PerCP-Cy5.5 (BD Pharmingen, 564718). For p53 analysis, after permeabilization cells were incubated with monoclonal anti-phosphate p53 (Ser15) antibody (clone D4S1H) (Cell Signaling Technologies, 12571), then washed and incubated with Alexa Fluor 488 goat anti-rabbit immunoglobulin G (Life Technologies, A11034). Samples were analyzed on a FACSCanto analyzer (BD Bioscience).

RNA Preparation and Transcriptome Analysis

RNA of sorted cells was purified using an RNeasy Plus Micro Kit (Qiagen) according to manufacturer's protocol. In brief, cells were lysed in RLT Plus buffer supplemented with 10^{-4} M β-mercaptoethanol, and DNA was removed using a gDNA Eliminator spin column. RNA was purified using an RNeasy column, eluted in RNase-free water, and stored at −80°C. RNA was used for transcriptomic assay or real-time qRT-PCR assay (Supplemental Experimental Procedures). RNA concentration and integrity were evaluated with the Agilent Bioanalyzer 2100. Affymetrix Mouse Gene MTA1.0 and Hu-Gene 2.0 ST arrays were respectively used for mouse and human samples. Supervised analyses were performed to identify genes specifically up- or downregulated in *Fancg*$^{-/-}$ or FA HSCs, and lists of differentially expressed genes were analyzed for GO with DAVID (database used for annotation, visualization, and integrated discovery) (http://david.abcc.ncifcrf.gov), KEGG (Kyoto Encyclopedia of Genes and Genomes) pathway, and reactome analyses. The global expression profile was also analyzed with GSEA with the functional (curated) dataset present in the Molecular Signature Database of the Broad Institute (www.broadinstitute.org/gsea) (Subramanian et al., 2005). An anti-correlation study was performed using R. M values (or $\log_2$(FC) between *Fancg*$^{-/-}$ and WT) of E14.5 was plotted against M values of E12.5, and Pearson correlation coefficient calculated.

Statistical Analysis

Statistical analysis was performed using the Mann-Whitney, Wilcoxon, and χ^2 tests. $p < 0.05$ was considered significant. Data were expressed as mean or median ± SD.

ACCESSION NUMBERS

The GEO accession number for arrays reported in this paper is GEO: GSE120169.

SUPPLEMENTAL INFORMATION

Supplemental Information includes Supplemental Experimental Procedures, three figures, and three tables and can be found with this article online at https://doi.org/10.1016/j.stemcr.2018.10.001.

AUTHOR CONTRIBUTIONS

C.D. designed and performed experiments, and collected and analyzed data. L.M. performed experiments, collected and analyzed data. A.R., L.P., and S.S. performed experiments and collected data. D.C. performed cell sorting and set up cell-cycle analysis. S.J. performed the microarray gene expression experiment, and M.S., P.d.l.G., N.R., and F. Guidez performed analysis. F. Guimiot and J.S. provided human study material. M.P. and A.R. took care of the *Fancg*$^{-/-}$ core breeding and back cross. M.S.

and J.S. conceived the project. M.S. designed the study, performed data analysis, and provided financial support. M.S., C.D., and L.M. wrote the manuscript. All authors read and approved the final manuscript.

ACKNOWLEDGMENTS

We thank Christine Chomienne and Michele Goodhardt for critical reading of the manuscript and helpful discussions. Cell sorting by Hélène Fohrer-Ting at the cytometry platform of the Centre de Recherches des Cordeliers (Paris), and support by the animal core facilities of the Institut Universitaire d'Hématologie of the Saint-Louis Hospital and of the Institut de Biologie Paris Seine are gratefully acknowledged. This work was supported by INSERM (Institut National de la Santé et de la Recherche Médicale) and CNRS (Centre National de Recherche Scientifique) and by grants from INCA (Institut du Cancer), La Ligue contre le Cancer (Comité Ile-de-France), and AFMF (Association Française de la maladie de Fanconi). C.D. was a supported by fellowships from INSERM/INCA, APPEL (Association Philantropique des Parents des Enfants Leucémiques), and 111 des Arts.

Received: December 18, 2017
Revised: September 27, 2018
Accepted: October 1, 2018
Published: October 25, 2018

REFERENCES

Ayas, M., Saber, W., Davies, S.M., Harris, R.E., Hale, G.A., Socie, G., LeRademacher, J., Thakar, M., Deeg, H.J., Al-Seraihy, A., et al. (2013). Allogeneic hematopoietic cell transplantation for Fanconi anemia in patients with pretransplantation cytogenetic abnormalities, myelodysplastic syndrome, or acute leukemia. J. Clin. Oncol. *31*, 1669–1676.

Barroca, V., Mouthon, M.A., Lewandowski, D., Brunet de la Grange, P., Gauthier, L.R., Pflumio, F., Boussin, F.D., Arwert, F., Riou, L., Allemand, I., et al. (2012). Impaired functionality and homing of Fancg-deficient hematopoietic stem cells. Hum. Mol. Genet. *21*, 121–135.

Beerman, I., and Rossi, D.J. (2015). Epigenetic control of stem cell potential during homeostasis, aging, and disease. Cell Stem Cell *16*, 613–625.

Bluteau, D., Masliah-Planchon, J., Clairmont, C., Rousseau, A., Ceccaldi, R., Dubois d'Enghien, C., Bluteau, O., Cuccuini, W., Gachet, S., Peffault de Latour, R., et al. (2016). Biallelic inactivation of REV7 is associated with Fanconi anemia. J. Clin. Invest. *126*, 3580–3584.

Brosh, R.M., Jr., Bellani, M., Liu, Y., and Seidman, M.M. (2017). Fanconi anemia: a DNA repair disorder characterized by accelerated decline of the hematopoietic stem cell compartment and other features of aging. Ageing Res. Rev. *33*, 67–75.

Ceccaldi, R., Parmar, K., Mouly, E., Delord, M., Kim, J.M., Regairaz, M., Pla, M., Vasquez, N., Zhang, Q.S., Pondarre, C., et al. (2012). Bone marrow failure in Fanconi anemia is triggered by an exacerbated p53/p21 DNA damage response that impairs hematopoietic stem and progenitor cells. Cell Stem Cell *11*, 36–49.

Deans, A.J., and West, S.C. (2011). DNA interstrand crosslink repair and cancer. Nat. Rev. Cancer *11*, 467–480.

Dokal, I., and Vulliamy, T. (2008). Inherited aplastic anaemias/bone marrow failure syndromes. Blood Rev. *22*, 141–153.

Dong, H., Nebert, D.W., Bruford, E.A., Thompson, D.C., Joenje, H., and Vasiliou, V. (2015). Update of the human and mouse Fanconi anemia genes. Hum. Genomics *9*, 32.

Du, W., Amarachintha, S., Erden, O., Wilson, A., Meetei, A.R., Andreassen, P.R., Namekawa, S.H., and Pang, Q. (2015). Fancb deficiency impairs hematopoietic stem cell function. Sci. Rep. *5*, 18127.

Dumitriu, B., and Young, N.S. (2012). Damage control and its costs: BM failure in Fanconi anemia stems from overactive p53/p21. Cell Stem Cell *11*, 7–8.

Dzierzak, E., and Speck, N.A. (2008). Of lineage and legacy: the development of mammalian hematopoietic stem cells. Nat. Immunol. *9*, 129–136.

Ema, H., and Nakauchi, H. (2000). Expansion of hematopoietic stem cells in the developing liver of a mouse embryo. Blood *95*, 2284–2288.

Faivre, L., Guardiola, P., Lewis, C., Dokal, I., Ebell, W., Zatterale, A., Altay, C., Poole, J., Stones, D., Kwee, M.L., et al. (2000). Association of complementation group and mutation type with clinical outcome in fanconi anemia. European Fanconi Anemia Research Group. Blood *96*, 4064–4070.

Fitch, S.R., Kimber, G.M., Wilson, N.K., Parker, A., Mirshekar-Syahkal, B., Gottgens, B., Medvinsky, A., Dzierzak, E., and Ottersbach, K. (2012). Signaling from the sympathetic nervous system regulates hematopoietic stem cell emergence during embryogenesis. Cell Stem Cell *11*, 554–566.

Garaycoechea, J.I., and Patel, K.J. (2014). Why does the bone marrow fail in Fanconi anemia? Blood *123*, 26–34.

Gekas, C., Dieterlen-Lievre, F., Orkin, S.H., and Mikkola, H.K. (2005). The placenta is a niche for hematopoietic stem cells. Dev. Cell *8*, 365–375.

Gekas, C., Rhodes, K.E., Van Handel, B., Chhabra, A., Ueno, M., and Mikkola, H.K. (2010). Hematopoietic stem cell development in the placenta. Int. J. Dev. Biol. *54*, 1089–1098.

Greve, B., Bolling, T., Amler, S., Rossler, U., Gomolka, M., Mayer, C., Popanda, O., Dreffke, K., Rickinger, A., Fritz, E., et al. (2012). Evaluation of different biomarkers to predict individual radiosensitivity in an inter-laboratory comparison—lessons for future studies. PLoS One *7*, e47185.

Hays, L.E. (2012). A mismatched life in the stem cell pool. Blood *120*, 3164–3165.

Itoh, K., Tezuka, H., Sakoda, H., Konno, M., Nagata, K., Uchiyama, T., Uchino, H., and Mori, K.J. (1989). Reproducible establishment of hemopoietic supportive stromal cell lines from murine bone marrow. Exp. Hematol. *17*, 145–153.

Jordan, C.T., Astle, C.M., Zawadzki, J., Mackarehtschian, K., Lemischka, I.R., and Harrison, D.E. (1995). Long-term repopulating abilities of enriched fetal liver stem cells measured by competitive repopulation. Exp. Hematol. *23*, 1011–1015.

Kamimae-Lanning, A.N., Goloviznina, N.A., and Kurre, P. (2013). Fetal origins of hematopoietic failure in a murine model of Fanconi anemia. Blood *121*, 2008–2012.

Kelly, P.F., Radtke, S., von Kalle, C., Balcik, B., Bohn, K., Mueller, R., Schuesler, T., Haren, M., Reeves, L., Cancelas, J.A., et al. (2007). Stem cell collection and gene transfer in Fanconi anemia. Mol. Ther. *15*, 211–219.

Kim, K.H., and Sederstrom, J.M. (2015). Assaying cell cycle status using flow cytometry. Curr. Protoc. Mol. Biol. *111*, 28.6.1–28.6.11.

Kim, H., Yang, K., Dejsuphong, D., and D'Andrea, A.D. (2012). Regulation of Rev1 by the Fanconi anemia core complex. Nat. Struct. Mol. Biol. *19*, 164–170.

Knies, K., Inano, S., Ramirez, M.J., Ishiai, M., Surralles, J., Takata, M., and Schindler, D. (2017). Biallelic mutations in the ubiquitin ligase RFWD3 cause Fanconi anemia. J. Clin. Invest. *127*, 3013–3027.

Koomen, M., Cheng, N.C., van de Vrugt, H.J., Godthelp, B.C., van der Valk, M.A., Oostra, A.B., Zdzienicka, M.Z., Joenje, H., and Arwert, F. (2002). Reduced fertility and hypersensitivity to mitomycin C characterize Fancg/Xrcc9 null mice. Hum. Mol. Genet. *11*, 273–281.

Kottemann, M.C., and Smogorzewska, A. (2013). Fanconi anaemia and the repair of Watson and Crick DNA crosslinks. Nature *493*, 356–363.

Kumaravelu, P., Hook, L., Morrison, A.M., Ure, J., Zhao, S., Zuyev, S., Ansell, J., and Medvinsky, A. (2002). Quantitative developmental anatomy of definitive haematopoietic stem cells/long-term repopulating units (HSC/RUs): role of the aorta-gonad-mesonephros (AGM) region and the yolk sac in colonisation of the mouse embryonic liver. Development *129*, 4891–4899.

Kupfer, G.M. (2013). Fanconi anemia: a signal transduction and DNA repair pathway. Yale J. Biol. Med. *86*, 491–497.

Kutler, D.I., Singh, B., Satagopan, J., Batish, S.D., Berwick, M., Giampietro, P.F., Hanenberg, H., and Auerbach, A.D. (2003). A 20-year perspective on the International Fanconi anemia registry (IFAR). Blood *101*, 1249–1256.

Medvinsky, A., Rybtsov, S., and Taoudi, S. (2011). Embryonic origin of the adult hematopoietic system: advances and questions. Development *138*, 1017–1031.

Mendelson, A., and Frenette, P.S. (2014). Hematopoietic stem cell niche maintenance during homeostasis and regeneration. Nat. Med. *20*, 833–846.

Mikkelsen, T.S., Ku, M., Jaffe, D.B., Issac, B., Lieberman, E., Giannoukos, G., Alvarez, P., Brockman, W., Kim, T.K., Koche, R.P., et al. (2007). Genome-wide maps of chromatin state in pluripotent and lineage-committed cells. Nature *448*, 553–560.

Mikkola, H.K., and Orkin, S.H. (2006). The journey of developing hematopoietic stem cells. Development *133*, 3733–3744.

Milyavsky, M., Gan, O.I., Trottier, M., Komosa, M., Tabach, O., Notta, F., Lechman, E., Hermans, K.G., Eppert, K., Konovalova, Z., et al. (2010). A distinctive DNA damage response in human hematopoietic stem cells reveals an apoptosis-independent role for p53 in self-renewal. Cell Stem Cell *7*, 186–197.

Morrison, S.J., Hemmati, H.D., Wandycz, A.M., and Weissman, I.L. (1995). The purification and characterization of fetal liver hematopoietic stem cells. Proc. Natl. Acad. Sci. U S A *92*, 10302–10306.

Muller, L.U., and Williams, D.A. (2009). Finding the needle in the hay stack: hematopoietic stem cells in Fanconi anemia. Mutat. Res. *668*, 141–149.

Nalepa, G., and Clapp, D.W. (2014). Fanconi anemia and the cell cycle: new perspectives on aneuploidy. F1000Prime Rep. *6*, 23.

Ottersbach, K., and Dzierzak, E. (2005). The murine placenta contains hematopoietic stem cells within the vascular labyrinth region. Dev. Cell *8*, 377–387.

Ottersbach, K., and Dzierzak, E. (2010). The placenta as a haematopoietic organ. Int. J. Dev. Biol. *54*, 1099–1106.

Park, J.Y., Virts, E.L., Jankowska, A., Wiek, C., Othman, M., Chakraborty, S.C., Vance, G.H., Alkuraya, F.S., Hanenberg, H., and Andreassen, P.R. (2016). Complementation of hypersensitivity to DNA interstrand crosslinking agents demonstrates that XRCC2 is a Fanconi anaemia gene. J. Med. Genet. *53*, 672–680.

Parmar, K., D'Andrea, A., and Niedernhofer, L.J. (2009). Mouse models of Fanconi anemia. Mutat. Res. *668*, 133–140.

Peffault de Latour, R., Porcher, R., Dalle, J.H., Aljurf, M., Korthof, E.T., Svahn, J., Willemze, R., Barrenetxea, C., Mialou, V., Soulier, J., et al. (2013). Allogeneic hematopoietic stem cell transplantation in Fanconi anemia: the European group for blood and marrow transplantation experience. Blood *122*, 4279–4286.

Petit-Cocault, L., Volle-Challier, C., Fleury, M., Peault, B., and Souyri, M. (2007). Dual role of Mpl receptor during the establishment of definitive hematopoiesis. Development *134*, 3031–3040.

Quentin, S., Cuccuini, W., Ceccaldi, R., Nibourel, O., Pondarre, C., Pagès, M.P., Vasquez, N., Dubois d'Enghien, C., Larghero, J., Peffault de Latour, R., et al. (2011). Myelodysplasia and leukemia of Fanconi anemia are associated with a specific pattern of genomic abnormalities that includes cryptic RUNX1/AML1 lesions. Blood *117*, e161–e170.

Ramkissoon, S.H., Patel, H.J., Taborga, M., and Rameshwar, P. (2006). G protein-coupled receptors in haematopoietic disruption. Expert Opin. Biol. Ther. *6*, 109–120.

Sanchez, M.J., Holmes, A., Miles, C., and Dzierzak, E. (1996). Characterization of the first definitive hematopoietic stem cells in the AGM and liver of the mouse embryo. Immunity *5*, 513–525.

Shim, J., Mukherjee, T., Mondal, B.C., Liu, T., Young, G.C., Wijewarnasuriya, D.P., and Banerjee, U. (2013). Olfactory control of blood progenitor maintenance. Cell *155*, 1141–1153.

Soulier, J. (2011). Fanconi anemia. Hematology Am. Soc. Hematol. Educ. Program *2011*, 492–497.

Subramanian, A., Tamayo, P., Mootha, V.K., Mukherjee, S., Ebert, B.L., Gillette, M.A., Paulovich, A., Pomeroy, S.L., Golub, T.R., Lander, E.S., et al. (2005). Gene set enrichment analysis: a knowledge-based approach for interpreting genome-wide expression profiles. Proc. Natl. Acad. Sci. U S A *102*, 15545–15550.

Suzuki, S., Racine, R.R., Manalo, N.A., Cantor, S.B., and Raffel, G.D. (2017). Impairment of fetal hematopoietic stem cell function in the absence of Fancd2. Exp. Hematol. *48*, 79–86.

Tavian, M., and Peault, B. (2005). Embryonic development of the human hematopoietic system. Int. J. Dev. Biol. *49*, 243–250.

Tischkowitz, M., and Dokal, I. (2004). Fanconi anaemia and leukaemia - clinical and molecular aspects. Br. J. Haematol. *126*, 176–191.

Tulpule, A., Lensch, M.W., Miller, J.D., Austin, K., D'Andrea, A., Schlaeger, T.M., Shimamura, A., and Daley, G.Q. (2010). Knockdown of Fanconi anemia genes in human embryonic stem cells reveals early developmental defects in the hematopoietic lineage. Blood *115*, 3453–3462.

Walter, D., Lier, A., Geiselhart, A., Thalheimer, F.B., Huntscha, S., Sobotta, M.C., Moehrle, B., Brocks, D., Bayindir, I., Kaschutnig, P., et al. (2015). Exit from dormancy provokes DNA-damage-induced attrition in haematopoietic stem cells. Nature *520*, 549–552.

Yoon, Y.M., Storm, K.J., Kamimae-Lanning, A.N., Goloviznina, N.A., and Kurre, P. (2016). Endogenous DNA damage leads to p53-independent deficits in replicative fitness in fetal murine Fancd2$^{-/-}$ hematopoietic stem and progenitor cells. Stem Cell Reports *7*, 840–853.

Zhang, Q.S., Benedetti, E., Deater, M., Schubert, K., Major, A., Pelz, C., Impey, S., Marquez-Loza, L., Rathbun, R.K., Kato, S., et al. (2015). Oxymetholone therapy of fanconi anemia suppresses osteopontin transcription and induces hematopoietic stem cell cycling. Stem Cell Reports *4*, 90–102.

Zhang, H., Kozono, D.E., O'Connor, K.W., Vidal-Cardenas, S., Rousseau, A., Hamilton, A., Moreau, L., Gaudiano, E.F., Greenberger, J., Bagby, G., et al. (2016). TGF-β inhibition rescues hematopoietic stem cell defects and bone marrow failure in Fanconi anemia. Cell Stem Cell *18*, 668–681.

Stem Cell Reports, Volume *11*

Supplemental Information

Studies in an Early Development Window Unveils a Severe HSC Defect in both Murine and Human Fanconi Anemia

Carine Domenech, Loïc Maillard, Alix Rousseau, Fabien Guidez, Laurence Petit, Marika Pla, Denis Clay, Fabien Guimiot, Sandra Sanfilippo, Sebastien Jacques, Pierre de la Grange, Noémie Robil, Jean Soulier, and Michèle Souyri

Supplemental Information

Studies in an early development window unveil a severe HSC defect in both murine and human Fanconi anemia

Carine Domenech[1,2,3,4,5], Loïc Maillard[1,2,3,4], Alix Rousseau[4,6], Fabien Guidez[3,4], Laurence Petit[1,2], Marika Pla[3,4], Denis Clay[7,8], Fabien Guimiot[9], Sandra Sanfilippo[1,2,10], Sebastien Jacques[11], Pierre de la Grange[12], Noémie Robil[12], Jean Soulier[4,6] and Michèle Souyri*[1,2,3,4]

Inventory of Supplemental Informations

- **Table S1, related to Figure 6 and transcriptome analysis section in the Results,** reports all the GO processes and genes associated (DAVID, KEGG and reactome analysis) in genes in *Fancg*$^{-/-}$ E12.5 Pl and E14.5 FL and human FA FL HSCs.
- **Table S2, related to Figure 6 and transcriptome analysis section in the Results,** shows expression of few cell cycle regulators in E12.5 FL and E14.5 FL *Fancg*$^{-/-}$ HSCs and in human FA FL HSCs.
- **Table S3, related to Figure 6 and transcriptome analysis section in the Results,** shows transcriptional regulators and markers important for HSC development and maintenance in E12.5 FL and E14.5 FL *Fancg*$^{-/-}$ HSCs and in human FA FL HSCs.

- **Figure S1, related to Figure 2,** shows that the percentage of HSC-enriched cells in *Fancg*$^{-/-}$ E12.5 Pl or FL, and E14.5 FL is identical to that detected in WT Pl or FL.
- **Figure S2, related to Figure 3,** reports long-term primary and secondary hematopoietic reconstitution ability of E14.5 FL LSA HSCs.
- **Figure S3,** reports analysis of apoptosis in *Fancg*$^{-/-}$ and WT E12.5 FL LSA HSC population **(related to Figure 4)**, and qPCR verification of the level of expression of few cell cycle and HSC-related genes **(related to Figure 6 and Tables S2 and S3)**, and analysis of phospho-P53 in HCs and HSCs populations from *Fancg*$^{-/-}$ and WT E12.5 FL **(related to Table S2)**.

Supplemental Figures and Legends

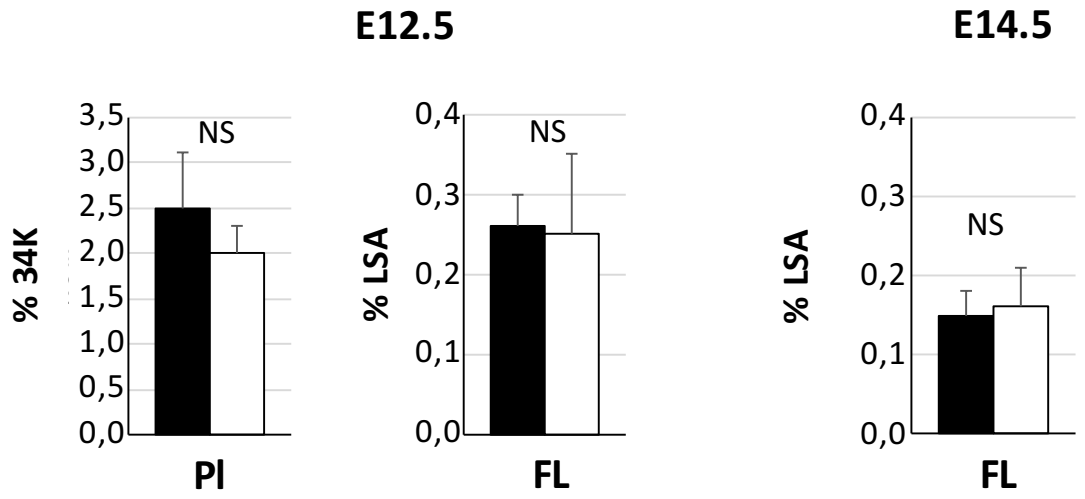

Figure S1. Related to Figure 2. Percentage of HSC-enriched populations.
Percentage of HSC-enriched cells in the Pl (34K, n=9 - distinct experiments) and FL (LSA, n=7 - distinct experiments) at E12.5 and in the FL (LSA, n=6 - distinct experiments) at E14.5.
Black bars: WT; White bars: *Fancg*$^{-/-}$.
NS: not significant.
Error bars correspond to standard deviation (SD).

A.

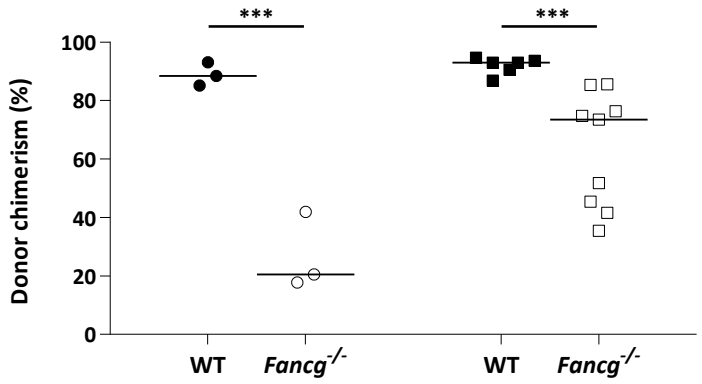

	1000 LSA FL		5000 LSA FL	
REC mice (%)	100	100	100	100
Median engrafment (%)	86.8	20.5	93	73.5

B.

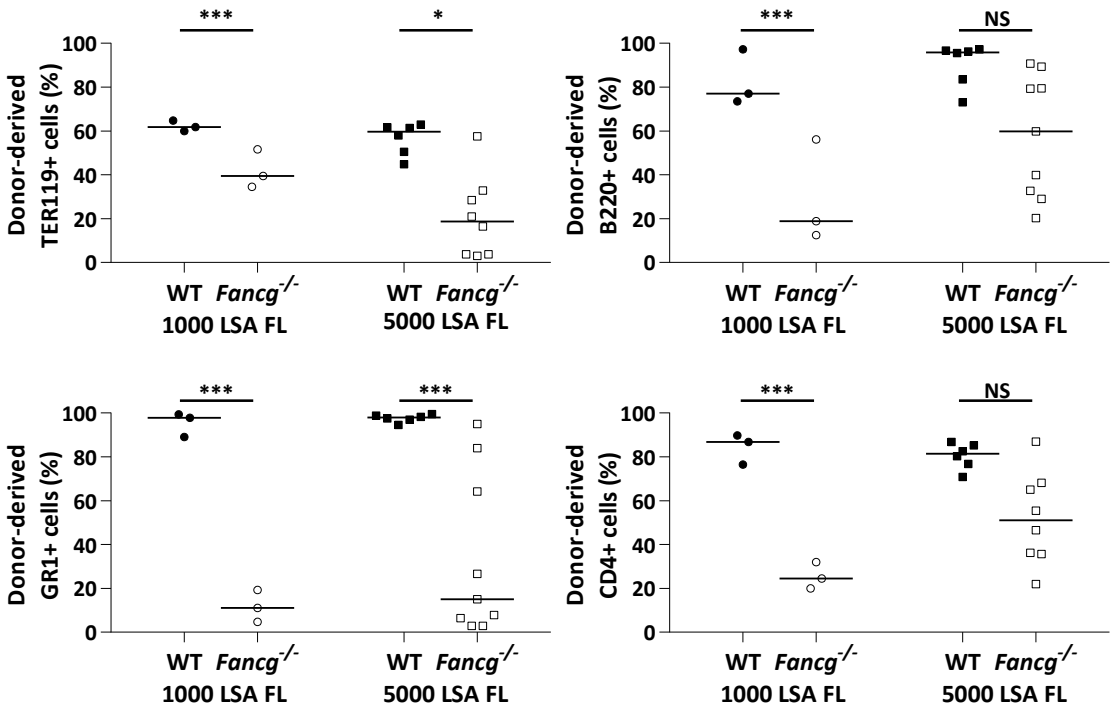

C.

Primary Transplantation		Secondary Transplantation		
		N° BM cells injected	Engrafted mice / Total mice	Median reconstitution (%) [Lower rec – Higher rec]
E14.5 FL	WT	$0.5x10^6$	4/4	72.3 [65.8-74]
	Fancg$^{-/-}$	$2x10^6$	3/4	7.7 [6.8-11]

Figure S2. Related to Figure 3. High LTR ability defect and impaired myeloid potential of E14.5 *Fancg*$^{-/-}$ FL LSA HSCs. (A) CD45.2 chimerism in the blood of primary recipients 16- to 20-week post injection of 1.10^3 (circles) or 5.10^3 (squares) WT (black) or *Fancg*$^{-/-}$ (white) LSA cells. (B) Analysis of the BM hematopoietic content of primary recipients transplanted with LSA cells, expressed as a percentage of CD45.2$^+$ erythroid (TER119), myeloid (GR1), B lymphoid (B220) and T-lymphoid (CD4) cells. Circles: 1.10^3 LSA injected; squares: 5.10^3 LSA injected; black: WT FL or Pl cells; White: *Fancg*$^{-/-}$ FL or Pl cells. (C) Secondary transplantations. Engraftment was considered as positive when CD45.2 chimerism in the blood was >5%.
*** $p<0.001$; * $p<0.05$; NS: not significant.

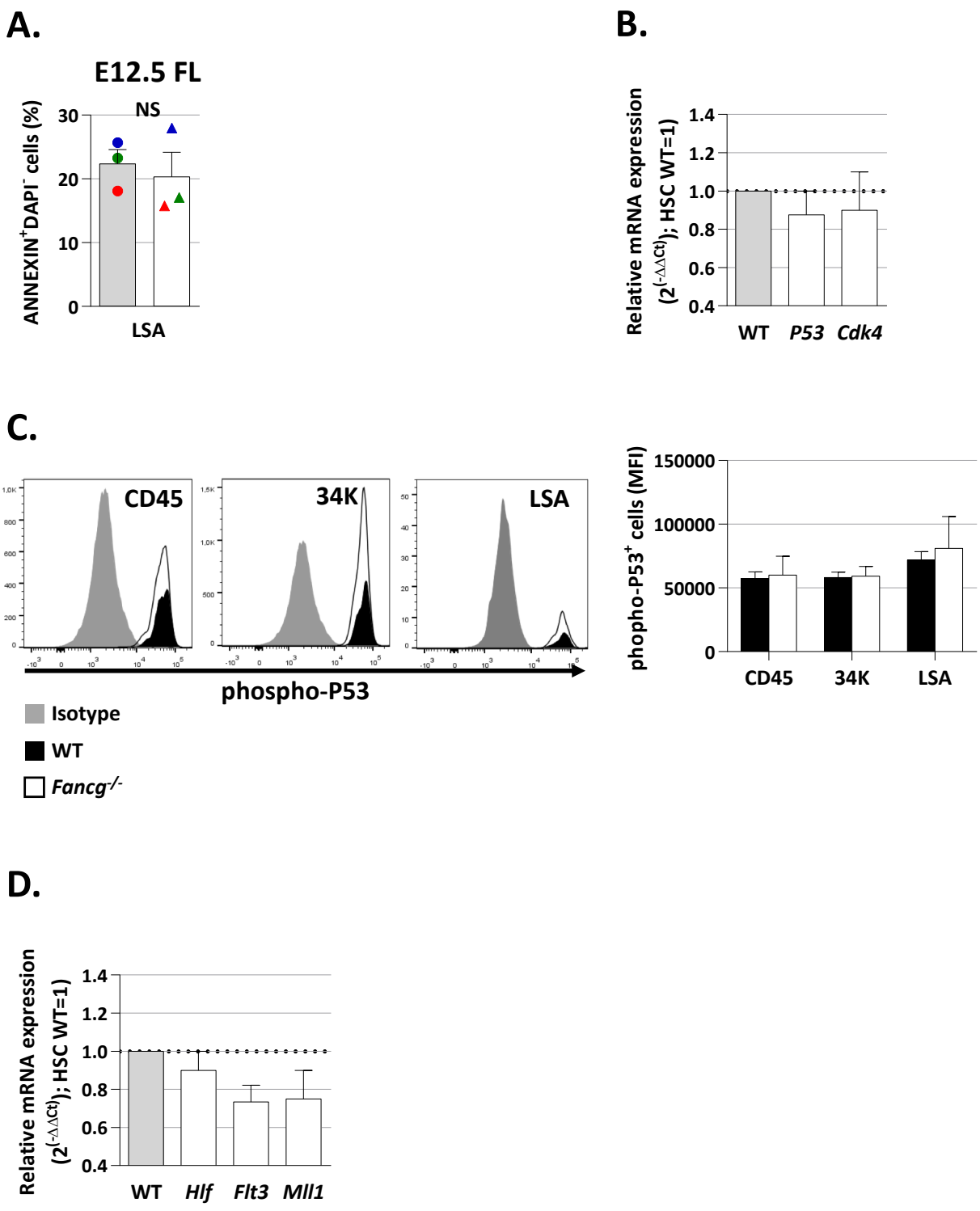

Figure S3. Related to Figure 4 and Figure 6. Annexin, p53, and qPCR. (A) ANNEXIN^{+}DAPI^{-} LSA cells in E12.5 FL (n=3, dots of same colors are related to the same experiment), measured by flow-cytometry. Grey bars: WT; White bars: Fancg$^{-/-}$. NS: not significant. (B, D) qPCR of relative mRNA expression of (B) cell cycle related genes (*P53*, *Cdk4*) and (D) HSC related genes (*Hlf*, *Flt3*, *Mll1*) in E12.5 FL HSCs. Grey bars: WT; White bars: Fancg$^{-/-}$. (C) Left panel, histograms of phospho-P53 expression in CD45^{+}, 34K and LSA in E12.5 FL. Right panel, MFI of phospho-P53 in CD45^{+}, 34K and LSA in E12.5 FL. Grey: Isotype; Black: WT; White: Fancg$^{-/-}$, n=3. Error bars correspond to standard deviation (SD).

Supplemental Tables

Table S1. Related to Figure 6. GO processes for up- and down-regulated genes in *Fancg*$^{-/-}$ E12.5 Pl and E14.5 FL and human FA FL HSCs determined by DAVID, KEGG and Reactome pathways (excel file).

Table S2. Related to Figure 6. Expression of cell cycle regulators in E12.5 FL and E14.5 FL *Fancg*$^{-/-}$ HSCs and in human FA FL HSCs

	MOUSE			E12.5 FL HSC *Fancg*$^{-/-}$vs WIE14.5 FL HSC *Fancg*$^{-/-}$vs WT				HUMAN		Hu FL CSH FA vs N	
	EntrezGeneID	Symbol	Type(s)	p-value	Fold-Change	p-value	Fold-Change	EntrezGene ID	Symbol	p-value	Fold-Change
positive regulators cell cycle	12534	***Cdk1***	kinase (G2/M)	0.0265882	-1.95099	*0.523601*	1.19537	983	***CDK1***	0.049633	-2.34181
	12566	***Cdk2***	kinase (G1/S and S)	*0.244252*	-1.47903	*0.861626*	1.05902	1017	***CDK2***	0.0286387	-1.50515
	12567	***Cdk4***	kinase (G1)	0.061724	-2.40922	*0.638159*	1.23345	1019	***CDK4***	*0.13786*	1.44103
	12571	***Cdk6***	kinase (G1)	*0.068171*	-2.01864	*0.624994*	1.196	1021	***CDK6***	*0.413603*	-2.13399
	12530	***Cdc25a***	phosphatase	*0.0707752*	-2.0569	*0.256828*	1.54979	993	***CDC25A***	*0.899374*	-1.11772
positive regulators G1/S	12545	***Cdc7***	kinase	0.00571329	-1.52194	*0.278122*	1.15937	8317	***CDC7***	0.0184651	-10.022
	72391	***Cdkn3***	phosphatase	0.0123337	1.80254	*0.163852*	-1.35654	1033	***CDKN3***	*0.163052*	-4.89689
	26965	***Cul1***	enzyme	*0.940323*	1.02756	*0.865013*	1.06371	8454	***CUL1***	0.0227364	-2.8474
	26554	***Cul3***	enzyme	*0.0762675*	-1.38092	*0.81476*	-1.04139	8452	***CUL3***	0.00796146	-8.41682
	27214	***Dbf4***	kinase	*0.100316*	-1.58151	*0.48082*	-1.20889	10926	***DBF4***	*0.422796*	-1.40464
	27401	***Skp2***	enzyme	*0.29602*	-1.32127	*0.505338*	1.19212	6502	***SKP2***	0.0341479	-1.60341
negative regulators G1 and G1/S	12575	***Cdkn1a (p21)***	kinase	*0.19388*	-1.29206	0.00169713	2.03639	1026	***CDKN1A***	*0.627505*	1.69843
	12576	***Cdkn1b (p27)***	kinase	*0.242822*	-1.33249	*0.933519*	-1.01964	1027	***CDKN1B***	*0.269765*	-1.56777
	12577	***Cdkn1c (p57)***	other	*0.976823*	-1.0031	*0.0818228*	-1.21492	1028	***CDKN1C***	0.0528907	1.40915
	12578	***Cdkn2a (p16)***	transcription regulator	0.0138273	1.51116	*0.481858*	-1.11356	1029	***CDKN2A***	0.0579896	1.67837
	12580	***Cdkn2c (p18)***	transcription regulator	*0.169685*	1.64242	*0.78489*	1.10051	1031	***CDKN2C***	*0.993546*	-1.00365
	12581	***Cdkn2d (p19)***	transcription regulator	*0.328384*	-1.68009	*0.901609*	1.06678	1032	***CDKN2D***	*0.163026*	1.95938
DNA Damage Response	22059	***Tp53***	transcription regulator	0.020398	-2.28048	*0.329335*	1.38025	7157	***TP53***	0.0357746	-4.79119
	12649	***Chek1***	kinase	*0.101596*	-1.71194	*0.62796*	1.16524	1111	***CHEK1***	*0.476714*	-1.3565
	11920	***Atm***	kinase	0.0196423	-1.36019	*0.235506*	1.15751	472	***ATM***	0.0146579	-4.59635
	245000	***Atr***	kinase	*0.295867*	-1.155	*0.155405*	1.21996	545	***ATR***	*0.0882164*	-2.72483
	26416	***Mapk14***	kinase	*0.100101*	-1.78115	*0.870933*	-1.05612	1432	***MAPK14***	*0.155265*	-1.71515

italics : p-value >0.05

Table S3. Related to Figure 6. Expression of transcriptional regulators and markers important for HSC development and maintenance in E12.5 FL and E14.5 FL *Fancg*$^{-/-}$ HSCs and in human FA FL HSCs

MOUSE			E12.5 FL HSC Fancg$^{-/-}$ vs WT		E14.5 FL HSC Fancg$^{-/-}$ vs WT		HUMAN		Hu FL HSC FA vs N	
EntrezGeneID	Symbol	Type(s)	p-value	Fold-Change	p-value	Fold-Change	Entrez Gene ID	Symbol	p-value	Fold-Change
17863	***Myb***	transcription regulator	*0.551193*	-1.26695	*0.764629*	1.12565	4602	***MYB***	*0.72529*	-1.82171
14461	***Gata2***	transcription regulator	0.000671183	-1.63055	*0.139091*	1.19841	2624	***GATA2***	*0.839851*	1.55964
15405	***Hoxa9***	transcription regulator	*0.791312*	1.04128	*0.132993*	-1.2687	3205	***HOXA9***	0.0187017	3.59795
217082	***Hlf***	transcription regulator	0.00182585	-1.94873	*0.394645*	-1.16941	3131	***HLF***	*0.400577*	-1.89707
17268	***Meis1***	transcription regulator	0.00111461	-1.83682	*0.253189*	1.19943	4211	***MEIS1***	*0.209917*	-2.5383
16909	***Lmo2***	transcription regulator	0.041514	-1.67244	*0.74554*	1.07963	4005	***LMO2***	0.0156993	-1.60739
12394	***Runx1***	transcription regulator	0.0226876	-2.04944	*0.196683*	1.46733	861	***RUNX1***	*0.77931*	-1.62861
21349	***Tal1***	transcription regulator	*0.876997*	-1.03302	*0.826557*	-1.04709	6886	***TAL1***	0.013999	-1.40094
14056	***Ezh2***	transcription regulator	*0.242662*	-1.2982	*0.851762*	1.0417	2146	***EZH2***	*0.0680242*	-1.86875
12393	***Runx2***	transcription regulator	*0.0705636*	-1.26931	*0.69666*	1.05007	860	***RUNX2***	*0.427646*	-1.71222
14011	***Etv6***	transcription regulator	0.0481506	-2.1165	*0.703837*	1.14525	2120	***ETV6***	*0.149461*	-3.75014
13876	***Erg***	transcription regulator	0.00811629	-2.00213	*0.651597*	-1.11153	2078	***ERG***	*0.951723*	1.02782
17128	***Smad4***	transcription regulator	0.00303934	-2.15952	*0.6264*	1.11578	4089	***SMAD4***	*0.0758063*	-3.40223
21423	***Tcf3 (E2a)***	transcription regulator	0.0101073	-1.85672	*0.409928*	1.19673	6929	***TCF3 (E2A)***	*0.976242*	-1.00542
20230	***Satb1***	transcription regulator	0.0000373983	-1.9032	*0.188524*	-1.13722	6304	***SATB1***	0.0455969	-2.32733
14247	***Fli1***	transcription regulator	0.0210975	-2.09813	*0.600603*	1.16741	2313	***FLI1***	*0.305429*	-1.83813
17480	***Mpl***	transmembrane receptor	0.00652311	-2.59841	*0.934073*	-1.02601	4352	***MPL***	*0.772362*	-1.70948
16590	***Kit***	transmembrane receptor	0.00876411	-2.15246	*0.996552*	1.00113	3815	***KIT***	0.0279414	-5.30959
14255	***Flt3***	kinase	0.0000856308	-3.26137	*0.678667*	1.10044	2322	***FLT3***	0.0150671	-11.4272
12490	***CD34***	other	0.0296424	-1.77092	*0.578961*	1.1452	947	***CD34***	*0.291241*	-2.26558
17064	***CD93***	other	0.0492916	-1.5755	*0.732869*	1.07704	22918	***CD93***	*0.743419*	-1.30972
12767	***Cxcr4***	G-protein coupled recep	0.0453386	-2.00912	*0.883063*	1.04921	7852	***CXCR4***	0.00546894	-2.60175
110454	***Ly6a (Sca1)***	other	0.525021	-1.17961	*0.869235*	-1.04344				
13435	***Dnmt3A***	enzyme	0.0000019344	-1.81074	0.0054889	1.30033	1788	***DNMT3A***	*0.194286*	-2.16926
13436	***Dnmt3B***	enzyme	0.00615053	-3.07848	*0.313957*	1.44877	1789	***DNMT3B***	*0.545676*	-1.53146
269966	***NUP98***	transporter	*0.163985*	-1.71656	*0.819614*	1.08966	4928	***NUP98***	*0.237552*	-2.46241
380669	***Lin28b***	other	0.0117365	-2.11293	*0.377657*	1.26962	389421	***LIN28B***	*0.414911*	-2.09804
15364	***Hmga2***	enzyme	0.0219313	-1.54098	*0.191152*	1.26183	8091	***HMGA2***	0.0138053	-3.28699

italics : p-value > 0.05

Supplemental Experimental Procedures

RT-qPCR

For RT-qPCR assay, RNA were reverse-transcripted in cDNA using SuperScript III Reverse Transcriptase kit (Invitrogen) according to manufacturer's protocol. qPCR was done using SYBR Green PCR master mix reagent (Applied Biosystems) on 7500 Fast RTPCR system (Applied Biosystems). Primers used for RT-qPCR assay are listed below.

Target	Sens	Primers 5'-3'
Cell cycle markers		
P53	Forward	GAGGCCGGCTCTGAGTATACCA
	Reverse	GGCAGGCACAAACACGAACC
Cdk4	Forward	CGGCCTGTGTCTATGGTCTG
	Reverse	GAAGCAGGGGATCTTACGCT
HSCs markers		
Hlf	Forward	GCAGCCGTCTACGTTTTCAA
	Reverse	CAGGATGCTTTCTCACCTGC
Flt3	Forward	TGTCAGTAATGATTCTTGAGACCGT
	Reverse	GCACACTGGAGGTCTTCTGG
Mll1	Forward	GGCCCTGTTGAATTCTCGGA
	Reverse	GGGAGCTTCGGGAAGGTATG
Gapdh	Forward	AGGTCGGTGTGAACGGATTTG
	Reverse	TGTAGACCATGTAGTTGAGGTCA